Second order average Hamiltonian theory of symmetry-based pulse schemes in the nuclear magnetic resonance of rotating solids: Application to triple-quantum dipolar recoupling

Andreas Brinkmann
Physical Chemistry/Solid State NMR, NSRIM Center, University of Nijmegen, Toernooiveld 1, 6525 ED Nijmegen, The Netherlands

Mattias Edén[a)]
Physical Chemistry Division, Arrhenius Laboratory, Stockholm University, SE-106 91 Stockholm, Sweden

(Received 22 December 2003; accepted 17 March 2004)

The average Hamiltonian theory (AHT) of several classes of symmetry-based radio-frequency pulse sequences is developed to second order, allowing quantitative analyses of a wide range of recoupling and decoupling applications in magic-angle-spinning solid state nuclear magnetic resonance. General closed analytical expressions are presented for a cross term between any two interactions recoupled to second order AHT. We classify them into different categories and show that some properties of the recoupling pulse sequence may be predicted directly from this classification. These results are applied to examine a novel homonuclear recoupling strategy, effecting a second order average dipolar Hamiltonian comprising trilinear triple quantum (3Q) spin operators. We discuss general features and design principles of such 3Q recoupling sequences and demonstrate by numerical simulations and experiments that they provide more efficient excitation of ^{13}C 3Q coherences compared to previous techniques. We passed up to 15% of the signal through a state of 3Q coherence in rotating powders of uniformly ^{13}C-labeled alanine and tyrosine. Second order recoupling-based ^{13}C homonuclear 3Q correlation spectroscopy is introduced and demonstrated on tyrosine. [DOI: 10.1063/1.1738102]

I. INTRODUCTION

One reason for the success of solid state nuclear magnetic resonance (NMR) in determining molecular structure and dynamics is the high control offered to selectively preserve and suppress various nuclear spin interactions during the experiment.[1–3] The manipulations may broadly be classified into recoupling, decoupling and preservation of a given interaction.

Decoupling leads to spin dynamics in the absence of a given interaction Hamiltonian. One example is magic-angle spinning (MAS), carried out by rapid rotation of the sample at the ''magic angle'' ($\theta_m = \arctan\sqrt{2}$) with respect to the external magnetic field direction. MAS averages out anisotropic interactions transforming under rotations as second rank tensors, e.g., chemical shift anisotropies (CSA) and dipolar couplings. *Recoupling*,[4,5] usually effected by application of radio-frequency (rf) pulses, selectively recovers a certain anisotropy under MAS conditions but may also involve the transformation of an interaction into a form different from its initial high-field spin Hamiltonian. An example is in multiple-quantum (MQ) NMR on spins-1/2,[6–8] which usually employs a dipolar Hamiltonian comprising double-quantum (2Q) spin operators (S^+S^+), whereas the high-field dipolar Hamiltonian is proportional to zero-quantum (ZQ) operators (S^-S^+).

In the framework of average Hamiltonian theory (AHT)[1,2] the spin dynamics is governed by a time-independent average Hamiltonian (AH), $\bar{H}$, representing the effective interaction resulting from the commensurate use of MAS and rf pulse sequences over a period T. Employing a perturbation order indexing starting at one[9–13] the average Hamiltonian may be expressed according to the Magnus expansion,[14]

$$\bar{H} = \bar{H}^{(1)} + \bar{H}^{(2)} + \bar{H}^{(3)} + \cdots \tag{1}$$

with the first two orders of perturbation given by

$$\bar{H}^{(1)} = \frac{1}{T}\int_{t_0^0}^{t_0^0+T} dt\, \tilde{H}(t), \tag{2}$$

$$\bar{H}^{(2)} = (2iT)^{-1}\int_{t_0^0}^{t_0^0+T} dt' \int_{t_0^0}^{t'} dt[\tilde{H}(t'),\tilde{H}(t)]. \tag{3}$$

Here t_0^0 denotes the start of the pulse sequence and $\tilde{H}(t)$ is an interaction frame Hamiltonian, related to the laboratory-frame Hamiltonian $H(t)$ by a unitary transformation induced by the rf pulses.

The present work focuses on the theoretical development and design of so-called symmetry-based RN_n^ν and CN_n^ν pulse sequences.[9,11–13,15–34] Such schemes directly exploit the unique response of each spin interaction to the combined modulations of MAS and rf pulses. The former transforms the spatial parts of the Hamiltonian, whereas the latter modulates its spin parts.[1–3] By choice of three integer symmetry

a)Author to whom correspondence should be addressed. Electronic mail: mattias@physc.su.se

numbers (N, n, ν) one can selectively recouple a given part of an interaction, while suppressing its other parts, as well as other interactions.[13] While the underlying AHT of symmetry-based pulse sequences is well-developed to first order AHT, allowing quantitative calculations of the size of the recoupled interactions,[11–13,15,19] it is currently *only qualitative to higher orders*. Here we extend the second order average Hamiltonian theory of symmetry-based schemes to *quantitative* evaluations of recoupled second order terms and develop a theoretical framework for *MQ phase cycles*[6,10,12,35] and their combination with phase inversion supercycles.[13,23] It may potentially be applied to analyze a wide range of symmetry-based recoupling and decoupling problems.

In most situations, the higher order Magnus expansion terms are undesirable and targets for decoupling.[1,2] Our results assist in dealing with such problems both by predicting the suppression of certain classes of terms up to second order AHT, as well as providing a quantitative assessment of the sizes of the remaining terms. However, here we adopt a different viewpoint in that certain *second order terms are desirable and actively recoupled*, thereby shifting the spotlight onto the second order, rather than first order average Hamiltonian. Along these ideas, building on similar approaches for order-selective MQC excitation in static samples,[6] we design triple-quantum (3Q) selective pulse sequences useful in the context of ^{13}C spins undergoing MAS. By this approach, a spin ensemble state of 3QC is created directly from equilibrium longitudinal magnetization.[35]

High-order MQC excitation involving ^{1}H spins under MAS conditions is fairly straightforward,[35–41] as the homonuclear dipolar interactions are dominant and chemical shift interactions are small. However, it is a challenging task for applications to less magnetic nuclei, e.g., ^{13}C, that additionally have a large spread of chemical shift interactions. Few reports exist of excitation of ^{13}C MQC of orders higher than two in samples undergoing MAS.[30,42–45] 3QC excitation exploiting ''second order recoupling'' requires tight control of the various terms of the Magnus expansion, as it demands efficient suppression of all dipolar and chemical shift contributions to first order; these terms are about an order of magnitude larger than the desired second order average Hamiltonian 3Q terms. This is achieved by $\mathrm{R}N_n^\nu$ or $\mathrm{C}N_n^\nu$ sequences combined with MQ phase cycles and phase inversion supercycles.

Despite the challenges encountered in the design of 3Q selective sequences, the reward is a highly efficient mechanism of 3QC excitation in powders: this is crucial since the NMR signal intensity is directly proportional to the triple-quantum filter (3QF) efficiency. Theoretically, about 55% of the total signal may be recovered in a triple-quantum filtration (3QF) experiment by this broadband approach. This is more than three times higher than offered by previous techniques for 3Q excitation among spins-1/2 under MAS conditions[30,42] and comparable to 2QF efficiencies from 2Q recoupling techniques in common use. Experimentally, we have passed 10–15% of the signal through 3QC in uniformly ^{13}C labeled amino acids, which is about three times larger than that achieved by the previously best broadband option,[42] and slightly higher than the result of a recently introduced 3Q *frequency-selective* excitation technique.[30]

This paper is organized as follows: Section II introduces the pulse sequences employed in this work. Section III presents the second order average Hamiltonian theory of these schemes from a general standpoint, which is subsequently applied in the context of 3Q recoupling in Sec. IV, where the 3Q average Hamiltonian and its resulting spin dynamics is derived and discussed. Section V describes the engineering and evaluation of 3Q recoupling sequences by numerical simulations, and the analytical predictions of Sec. IV are tested. In particular, we focus on numerical evaluations of one MQ phase cycle [denoted $(\mathrm{R}18_3^7)3^1$] and supercycles thereof under experimentally realistic scenarios, including the effects of chemical shift interactions and rf amplitude errors. Next follows an experimental section, where $(\mathrm{R}18_3^7)3^1$ is used for ^{13}C 3QC excitation in uniformly ^{13}C-labeled L-alanine and L-tyrosine and second order recoupling is demonstrated in the context of ^{13}C 3QC–1QC homonuclear correlation spectroscopy. The results are finally summarized in the concluding section.

II. PULSE SEQUENCES

We will build rf pulse schemes around two pulse sequence classes, denoted $\mathrm{R}N_n^\nu$ (Refs. 12, 13, and 19) and $\mathrm{C}N_n^\nu$.[11,13,15,16,18,46] They are defined by three integer ''symmetry numbers'' (N, n, ν) and a train of pulses $\mathcal{E}_q$ [see Fig. 1(a)], derived from a basic element $\mathcal{E}^0$ of duration $\tau_E = n\tau_r/N$, where $\tau_r = 2\pi/\omega_r$ is the rotational period and ω_r the spinning frequency. The two pulse sequence classes are distinguished by the properties of $\mathcal{E}^0$ and how the $\mathrm{R}N_n^\nu$ and $\mathrm{C}N_n^\nu$ sequence is built from the basic element. An $\mathrm{R}N_n^\nu$ scheme [Fig. 1(b)] is constructed from an inversion element $\mathcal{E}^0 \equiv \mathcal{R}$, i.e., a composite pulse effecting a net rotation of π around the rotating frame x axis. Another element $\mathcal{R}'$ may be generated from $\mathcal{R}$ by reversing the sign of all its rf phases. The $\mathrm{R}N_n^\nu$ scheme is formed by repeating the pair $\mathcal{R}_{\pi\nu/N}\mathcal{R}'_{-\pi\nu/N}$ $N/2$ times. A $\mathrm{C}N_n^\nu$ scheme, shown in Fig. 1(c), is built around a cyclic pulse train ($\mathcal{E}^0 \equiv \mathcal{C}$), meaning that in the absence of other spin interactions, the rf pulses of $\mathcal{C}$ return the spins to their original states at the completed element.[1] The $\mathrm{C}N_n^\nu$ sequence is obtained by concatenating N phase-shifted cycles, such that the qth element of the sequence, $\mathcal{C}_q$, has an overall phase shift $2\pi q\nu/N$. In the following, we will employ the shorthand notation $\mathcal{S} \equiv \mathrm{R}N_n^\nu$ or $\mathcal{S} \equiv \mathrm{C}N_n^\nu$. Given a sequence $\mathcal{S}$, $\mathcal{S}'$ is generated by reversing the sign of all phases within the basic element, as well as the sign of the symmetry number ν:[13,23,46] $\mathcal{S}' \equiv \mathrm{R}N_n^{-\nu}$ or $\mathcal{S}' \equiv \mathrm{C}N_n^{-\nu}$.

Generally, only a subset of the average Hamiltonian terms generated by $\mathcal{S}$ are desirable. The unwanted ones may be suppressed using supercycles, built from a concatenation of completed $\mathrm{R}N_n^\nu$ or $\mathrm{C}N_n^\nu$ sequences, combined according to certain patterns. Here we will exploit two such supercycle schemes: *MQ phase cycles*[6,10,35] [Fig. 1(d)] and *phase inversion supercycles*[13,23,46] [Fig. 1(e)]. An MQ phase cycle, $\mathcal{S}M^\chi$, closely resembles a $\mathrm{C}N_n^\nu$ sequence, with M replacing N and χ replacing ν: $\mathcal{S}M^\chi$ is constructed by concatenation of M phase-shifted sequences $\mathcal{S}_p$, such that the pth element has an

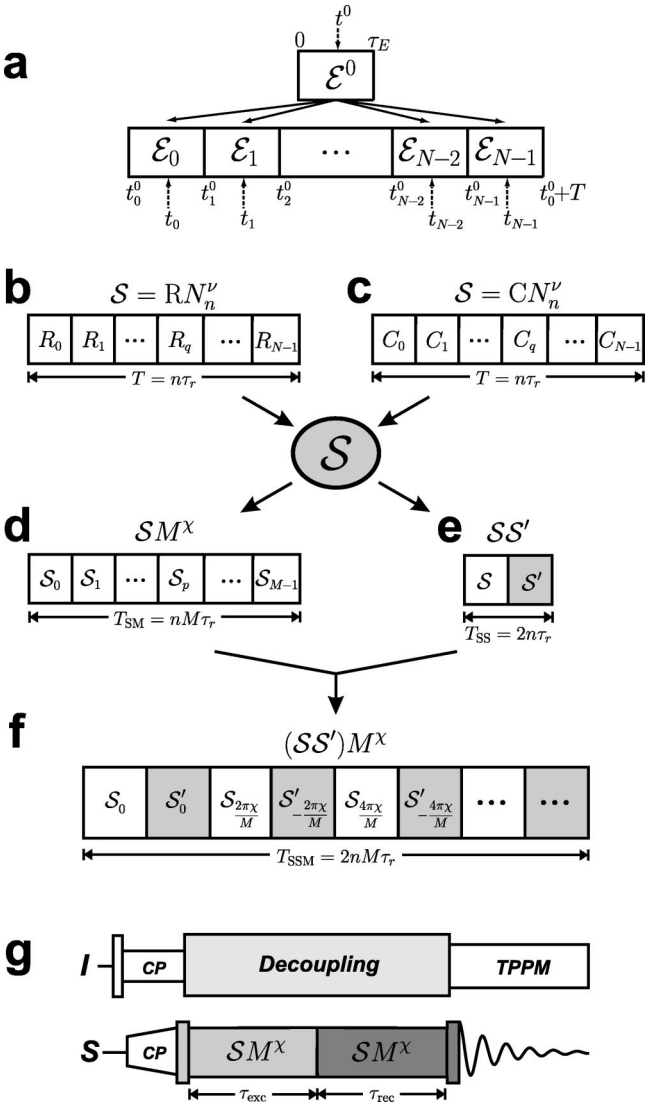

FIG. 1. The hierarchy of the various symmetry-based pulse schemes employed. (a) A general rotor-synchronized pulse sequence built of N elements $\mathcal{E}_0,\mathcal{E}_1,\ldots,\mathcal{E}_{N-1}$, derived from a basic element $\mathcal{E}^0$. The indicated time-points are discussed in Sec. III C 1: (b) $\mathrm{R}N_n^\nu$ sequence, (c) $\mathrm{C}N_n^\nu$ sequence. They are abbreviated $\mathcal{S}$ and used in supercycles, shown in (d)–(f). (d) The structure of an MQ phase cycle, $\mathcal{S}M^\chi$. (e) A phase inversion supercycle, $\mathcal{S}\mathcal{S}'$, where the sequence $\mathcal{S}'$ (shaded) is obtained by sign reversal of all phases of $\mathcal{S}$. (f) A nested MQ phase and inversion supercycle, $(\mathcal{S}\mathcal{S}')M^\chi$. (g) Pulse scheme for a triple-quantum filtration (3QF) experiment (Refs. 30, 35, and 42) incorporating an $\mathcal{S}M^\chi$ sequence for excitation and reconversion of 3QC.

overall phase shift $2\pi p\chi/M$, with $p=0,1,...,M-1$. The resulting MQ phase cycle extends over the interval $T_{SM}=nM\tau_r$. It is denoted $(\mathrm{R}N_n^\nu)M^\chi$ or $(\mathrm{C}N_n^\nu)M^\chi$, depending on the identity of $\mathcal{S}$. The only restriction is that $\mathcal{S}$ should be cyclic, which is fulfilled both by completed $\mathrm{R}N_n^\nu$ and $\mathrm{C}N_n^\nu$ sequences. A phase inversion supercycle constitutes the pair $\mathcal{S}\mathcal{S}'$, denoted $\mathrm{R}N_n^\nu\mathrm{R}N_n^{-\nu}$ and $\mathrm{C}N_n^\nu\mathrm{C}N_n^{-\nu}$ for $\mathcal{S}\equiv\mathrm{R}N_n^\nu$ or $\mathcal{S}\equiv\mathrm{C}N_n^\nu$, respectively.

Nested supercycles may be formed by combining MQ phase cycles and phase inversion supercycles.[13,23] The result of first forming a phase inversion sequence $\mathcal{S}\mathcal{S}'$ and subsequently applying MQ phase cycling is denoted $(\mathcal{S}\mathcal{S}')M^\chi$ and depicted in Fig. 1(f). It is constructed by applying an incrementing phase shift (reversed in sign for odd elements) to each element in a series of alternating sequences $\mathcal{S}$ and $\mathcal{S}'$,

$$(\mathcal{S}\mathcal{S}')M^\chi\equiv\mathcal{S}_0\mathcal{S}'_0\mathcal{S}_{2\pi\chi/M}\mathcal{S}'_{-(2\pi\chi/M)}\mathcal{S}_{4\pi\chi/M}\times\mathcal{S}'_{-(4\pi\chi/M)}\cdots\mathcal{S}_{[2\pi(M-1)\chi]/M}\mathcal{S}'_{[-2\pi(M-1)\chi]/M}. \tag{4}$$

This combination of MQ phase-cycling and phase-inversion supercycling is slightly different from that presented in Refs. 13 and 23, which corresponds to

$$[\mathcal{S}\mathcal{S}']_0[\mathcal{S}\mathcal{S}']_{2\pi\chi/M}[\mathcal{S}\mathcal{S}']_{4\pi\chi/M}\cdots[\mathcal{S}\mathcal{S}']_{[2\pi(M-1)\chi]/M}. \tag{5}$$

As discussed below, the two supercycles produce equivalent results in special cases, depending on the properties of the sequence $\mathcal{S}$.

III. THEORY

A. Spin interactions and Hamiltonians

The Hamiltonian H^Λ of a spin interaction Λ is a product of a component m of a lth rank spatial irreducible spherical tensor A^Λ, and a component μ of a λth rank spin irreducible spherical tensor operator T^Λ. The spin and spatial parts are denoted A^Λ_{lm} and $T^\Lambda_{\lambda\mu}$, respectively, with the components taking integer values in the range $-l\leqslant m\leqslant l$ and $-\lambda\leqslant\mu\leqslant\lambda$. The homonuclear dipolar interaction is second rank with respect to rotations, i.e., of its spatial and spin rank are $l=2$ and $\lambda=2$. Detailed classifications of the rotational symmetries of other spin interactions may be found in Refs. 1, 2, 13, and 47.

Restricting the analysis to coupled spins-1/2, the total laboratory-frame Hamiltonian is the sum over all spin interactions of the system and the rf Hamiltonian $H_{\mathrm{rf}}(t)$,

$$H(t)=H_{\mathrm{rf}}(t)+\sum_{\Lambda,\lambda,l,m}H^\Lambda_{lm\lambda0}(t), \tag{6}$$

$H_{\mathrm{rf}}(t)$ represents the rf field Hamiltonian and each spin Hamiltonian is uniquely specified by a quartet of integers (l,m,λ,μ) with the restriction $\mu=0$ in the high-field limit. Explicit expressions for the Hamiltonians may be found in Refs. 1, 2, 13, and 47. Each Hamiltonian term may be expressed as a product of a spin tensor component and a corresponding interaction frequency $\omega^\Lambda_{lm}(t)$,

$$H^\Lambda_{lm\lambda0}(t)=\omega^\Lambda_{lm}(t)T^\Lambda_{\lambda0} \tag{7}$$

with

$$\omega^\Lambda_{lm}(t)=[A^\Lambda_{lm}]^R d^l_{m0}(\beta_{RL})\exp\{-im(\alpha^0_{RL}-\omega_r t)\} \tag{8}$$

$[A^\Lambda_{lm}]^R$ is the mth component of the spatial tensor in a rotor frame R fixed on the sample holder. The z axis of this frame is inclined at the angle β_{RL} with respect to the static magnetic field direction; $\beta_{RL}=\arctan\sqrt{2}$ for exact magic-angle spinning. $d^l_{m0}(\beta)$ is a reduced Wigner element,[48] and α^0_{RL} defines the position of the rotor at time point $t=0$. The rotor-frame component of the interaction Λ is related to that in the principal axis system P by a sequence of rotations, involving an intermediate molecular frame M fixed on an arbitrary molecular fragment,

$$[A^{\Lambda}_{lm}]^R=\sum_{m',m''=-l}^{l}[A^{\Lambda}_{lm''}]^P D^{l}_{m''m'}(\Omega^{\Lambda}_{PM})d^{l}_{m'm}(\beta_{MR})\times\exp\{-i(m'\alpha_{MR}+m\gamma_{MR})\}. \quad (9)$$

In the case of the homonuclear $S-S$ through-space dipolar interaction between two spins j and k, only $[A^{jk}_{20}]^P=\sqrt{6}b_{jk}$ is nonzero, with the coupling constant b_{jk} related to the internuclear distance r_{jk} and the gyromagnetic ratio γ_S by $b_{jk}=-(\mu_0/4\pi)\gamma_S^2\hbar r_{jk}^{-3}$.

B. 3Q recoupling strategies

Here we outline our strategy for using the schemes of Fig. 1 in the context of homonuclear 3Q dipolar recoupling, assuming a system of (at least) three coupled spins-1/2 (labeled *i*, *j*, and *k*). The goal is to design a pulse sequence whose average dipolar Hamiltonian comprise *solely* the operators $T^{ijk}_{3\pm3}\sim S_i^{\pm}S_j^{\pm}S_k^{\pm}$, multiplied with a factor proportional to products of dipolar coupling constants. However, such *tri*linear spin operators may not be present in the first order average Hamiltonian $\bar{H}^{(1)}$ as it, according to Eq. (2), corresponds to the time average of a sequence of unitary transformations of the dipolar Hamiltonian, which itself is proportional to a *two*-spin operator $T_{2\mu}$. Nevertheless, the second order AH [Eq. (3)] may comprise trilinear spin operators, originating from commutators between spin operators from different pairs of couplings within the spin system, e.g., $[T^{ij}_{2+2},T^{ik}_{2+1}]\sim T^{ijk}_{3+3}$. Any pulse sequence generating such terms, among others, is referred to as giving *3Q recoupling*. If *only* 3Q operators are present (up to a certain order of the Magnus expansion) the sequence is referred to as being *3Q selective*. Hence, the aim of 3Q selective recoupling is to arrange that all first order AH contributions vanish, together with all terms in $\bar{H}^{(2)}$, except those resulting from commutators $[T^{ij}_{2\mu_2},T^{ik}_{2\mu_1}]$ obeying $\mu_1+\mu_2=\pm3$.

An MQ phase cycle $\mathcal{S}M^{\chi}$ restricts the average Hamiltonian to only comprise terms having spin operator components $\chi\mu$ being integral multiples of M.[6,35] The procedure is formally similar to coherence selection in NMR experiments,[49] but distinct in that the MQ phase cycling operates on the spin Hamiltonian instead of on the spin ensemble coherences. Hence, $\mathcal{S}3^{\pm1}$ schemes effect 3Q recoupling since $\bar{H}^{(2)}$ terms with $\mu_1+\mu_2=3Z$ (Z is any integer) are recoupled. However, because zero-quantum (ZQ) terms with $\mu_1+\mu_2=0$ are also symmetry allowed, the recoupling is *not* 3Q selective but $3Q/ZQ$ selective. The undesired ZQ terms may, however, be removed by a nested $(\mathcal{S}\mathcal{S}')3^{\pm1}$ scheme, a $(\mathcal{S}\mathcal{S}')3^{\pm1}$ scheme is 3Q selective to second order.

The following sections (III C–III F) give a *general* second order average Hamiltonian description of the various pulse schemes, subsequently applied to 3Q recoupling in Sec. IV.

C. Average Hamiltonian theory for CN^{ν}_{n} and RN^{ν}_{n} sequences

1. Interaction frame symmetry

The rotor-synchronized pulse sequence starts at time point t_0^0, as illustrated in Fig. 1(a). The qth element ($\mathcal{E}_q$) starts at t_q^0, and an arbitrary time point therein is denoted t_q ($t_q^0\leqslant t_q<t_{q+1}^0$), related to that within the *first* element through the time translation $t_q=t_0+q\tau_E$. Time points within the *basic* element $\mathcal{E}^0$ are denoted t^0, i.e., $0\leqslant t^0<\tau_E$, related to t_0 within the first element of the sequence by $t^0=t_0-t_0^0$.[12]

The rf propagator $U_{\rm rf}(t_q,t_0^0)$, active from the starting time point t_0^0 out to t_q within the qth element, may be expressed as three consecutive rotation operators $U_{\rm rf}(t_q,t_0^0)=R_z(\alpha_q)R_y(\beta_q)R_z(\gamma_q)$ involving three time dependent rf Euler angles $(\alpha_q,\beta_q,\gamma_q)=(\alpha(t_q),\beta(t_q),\gamma(t_q))$.[11–13,46] Analogously, the rf propagator from the starting time point $t=0$ of the basic element up to t^0 may be expressed $U_{\rm rf}(t^0,0)=R_z(\alpha^0)R_y(\beta^0)R_z(\gamma^0)$.

Prior to application of AHT, the spin interaction terms are transformed into the interaction frame of the rf field according to

$$\tilde{H}(t_q)=U_{\rm rf}(t_q,t_0^0)^{\dagger}H(t_q)U_{\rm rf}(t_q,t_0^0) \quad (10)$$

resulting in the following interaction frame Hamiltonian at time point t_q:

$$\tilde{H}(t_q)=\sum_{\Lambda,l,m,\lambda,\mu}\tilde{H}^{\Lambda}_{lm\lambda\mu}(t_q)=\sum_{\Lambda,l,m,\lambda,\mu}\tilde{\omega}^{\Lambda}_{lm\lambda\mu}(t_q)T^{\Lambda}_{\lambda\mu}. \quad (11)$$

Here $\tilde{\omega}^{\Lambda}_{lm\lambda\mu}(t_q)$ is given by[12]

$$\tilde{\omega}^{\Lambda}_{lm\lambda\mu}(t_q)=[A^{\Lambda}_{lm}]^R\exp\{-im\alpha^0_{RL}\}d^{l}_{m0}(\beta_{RL})\times d^{\lambda}_{\mu0}(-\beta_q)\exp\{i\mu\gamma_q+im\omega_r t_q\} \quad (12)$$

with the Euler angles $(\alpha_q,\beta_q,\gamma_q)$ related to the pulse sequence symmetry classes according to[12]

$$\beta_q=\begin{cases}\beta_0 & \text{for } CN^{\nu}_{n},\\ \beta_0+q\pi & \text{for } RN^{\nu}_{n},\end{cases} \quad (13)$$

$$\gamma_q=\gamma_0-\frac{2\pi\nu}{N}q. \quad (14)$$

Using the substitutions

$$\mathcal{Q}=\exp\{i2\pi Q/N\}, \quad (15)$$

$$Q=\begin{cases}mn-\mu\nu & \text{for } CN^{\nu}_{n},\\ mn-\mu\nu-\dfrac{\lambda N}{2} & \text{for } RN^{\nu}_{n},\end{cases} \quad (16)$$

the symmetry-based sequences impose the following interaction-frame time symmetry:

$$\tilde{\omega}^{\Lambda}_{lm\lambda\mu}(t_q)=\mathcal{Q}^q\tilde{\omega}^{\Lambda}_{lm\lambda\mu}(t_0). \quad (17)$$

Hence, the interaction frame frequency at the time point t_q within the qth pulse element of the sequence is related to t_0 within its *first* element by a simple exponential function involving the spin as well as spatial components and the symmetry numbers (N,n,ν) of the pulse scheme.

2. First order average Hamiltonian

In order to obtain a time-independent average Hamiltonian, we apply the Magnus expansion[14] to the interaction frame Hamiltonian Eq. (11). The first order AH is calculated from Eq. (2) giving

$$\overline{H}^{(1)}=\sum_{\Lambda,l,m,\lambda,\mu}\overline{H}^{\Lambda}_{lm\lambda\mu}=\sum_{\Lambda,l,m,\lambda,\mu}\overline{\omega}^{\Lambda}_{lm\lambda\mu}T^{\Lambda}_{\lambda\mu} \tag{18}$$

with

$$\overline{\omega}^{\Lambda}_{lm\lambda\mu}=T^{-1}\int_{t_0^0}^{t_0^0+T}dt\,\tilde{\omega}^{\Lambda}_{lm\lambda\mu}(t). \tag{19}$$

The periodicity in Eq. (17) allows expressing $\overline{\omega}^{\Lambda}_{lm\lambda\mu}$ according to

$$\overline{\omega}^{\Lambda}_{lm\lambda\mu}=S_{lm\lambda\mu}\kappa_{lm\lambda\mu}[A^{\Lambda}_{lm}]^{R}\exp\{-im(\alpha^0_{RL}-\omega_r t_0^0)\}, \tag{20}$$

where $\kappa_{lm\lambda\mu}$ is a scaling factor[13] of the recoupled term with quantum numbers (l,m,λ,μ). The sum $S_{lm\lambda\mu}$ only depends on the quantum numbers (l,m,λ,μ) and the symmetry numbers (N,n,ν) of the pulse sequence; it gives rise to the *first order selection rules* according to[11,13,15,19]

$$S_{lm\lambda\mu}=\frac{1}{N}\sum_{q=0}^{N-1}\mathcal{Q}^q=\begin{cases}0 & \text{if } \mathcal{Q}\neq 1\Leftrightarrow Q\neq NZ,\\ 1 & \text{if } \mathcal{Q}=1\Leftrightarrow Q=NZ,\end{cases} \tag{21}$$

where Z is any integer (including zero). Depending on the class of symmetry-based pulse sequence, they may be transformed to[11,13,15,19]

$$\overline{H}^{\Lambda}_{lm\lambda\mu}=S_{lm\lambda\mu}=0 \quad \text{if} \quad \begin{cases} mn-\mu\nu\neq NZ & \text{for } \mathrm{C}N^{\nu}_{n},\\ mn-\mu\nu\neq\dfrac{N}{2}Z_{\lambda} & \text{for } \mathrm{R}N^{\nu}_{n}.\end{cases} \tag{22}$$

Here Z_λ is an integer with the same parity as λ: for even λ, Z_λ represents any even integer, whereas it corresponds to any odd integer if λ is odd. The scaling factor $\kappa_{lm\lambda\mu}$ [Eq. (20)] depends on the quantum numbers (l,m,λ,μ) of the recoupled term, the type of pulse sequence ($\mathrm{C}N^{\nu}_{n}$ or $\mathrm{R}N^{\nu}_{n}$) and its symmetry numbers (N,n,ν), as well as on the pulses and phases of the basic pulse element $\mathcal{E}^0$,

$$\kappa_{lm\lambda\mu}=\begin{cases} d^{l}_{m0}(\beta_{RL})K_{m\lambda\mu} & \text{for } \mathrm{C}N^{\nu}_{n},\\ d^{l}_{m0}(\beta_{RL})\exp\left\{-i\mu\dfrac{\pi\nu}{N}\right\}K_{m\lambda\mu} & \text{for } \mathrm{R}N^{\nu}_{n}.\end{cases} \tag{23}$$

The factor $K_{m\lambda\mu}$ is defined with respect to the basic element $\mathcal{E}^0$ according to

$$K_{m\lambda\mu}=\tau_E^{-1}\int_0^{\tau_E}dt^0\,d^{\lambda}_{\mu 0}(-\beta^0)\exp\{i(\mu\gamma^0+m\omega_r t^0)\}, \tag{24}$$

where the symbols t^0, β^0, and γ^0 refer to time points and rf Euler angles within $\mathcal{E}^0$, defined explicitly in Ref. 12. The calculation of $K_{m\lambda\mu}$ for arbitrary elements $\mathcal{E}^0$ is discussed in Ref. 12 and extensions to second order scaling factor calculations are presented in the Appendix.

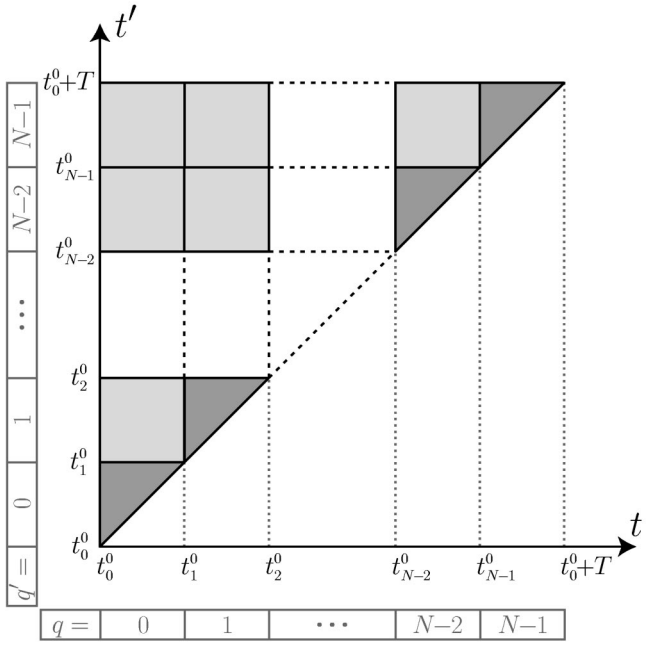

FIG. 2. The two-dimensional integration area of Eq. (27), with a selection of time points and the summation indices q and q' indicated.

3. Second order average Hamiltonian

The second order AH may be written

$$\overline{H}^{(2)}=\sum_{\substack{\Lambda_2,l_2,m_2,\lambda_2,\mu_2\\ \Lambda_1,l_1,m_1,\lambda_1,\mu_1}}\overline{H}^{\Lambda_2\times\Lambda_1}_{\substack{l_2m_2\lambda_2\mu_2\\ l_1m_1\lambda_1\mu_1}}, \tag{25}$$

where the sum is taken over all second order cross terms between a term of interaction Λ_2 with quantum numbers $(l_2,m_2,\lambda_2,\mu_2)$, and that of interaction Λ_1 with quantum numbers $(l_1,m_1,\lambda_1,\mu_1)$. The individual cross terms are given by

$$\overline{H}^{\Lambda_2\times\Lambda_1}_{\substack{l_2m_2\lambda_2\mu_2\\ l_1m_1\lambda_1\mu_1}}=\overline{\omega}^{\Lambda_2\times\Lambda_1}_{\substack{l_2m_2\lambda_2\mu_2\\ l_1m_1\lambda_1\mu_1}}[T^{\Lambda_2}_{\lambda_2\mu_2},T^{\Lambda_1}_{\lambda_1\mu_1}] \tag{26}$$

with the interaction frequencies

$$\overline{\omega}^{\Lambda_2\times\Lambda_1}_{\substack{l_2m_2\lambda_2\mu_2\\ l_1m_1\lambda_1\mu_1}}=(2iT)^{-1}\int_{t_0^0}^{t_0^0+T}dt'\int_{t_0^0}^{t'}dt\,\tilde{\omega}^{\Lambda_2}_{l_2m_2\lambda_2\mu_2}(t')\times\tilde{\omega}^{\Lambda_1}_{l_1m_1\lambda_1\mu_1}(t). \tag{27}$$

The range of the two-dimensional time integral is shown in Fig. 2. The symmetry relationship of the interaction-frame terms [Eq. (17)] leads to

$$\tilde{\omega}^{\Lambda_2}_{l_2m_2\lambda_2\mu_2}(t_{q'})\tilde{\omega}^{\Lambda_1}_{l_1m_1\lambda_1\mu_1}(t_q)=\mathcal{Q}_2^{q'}\mathcal{Q}_1^{q}\tilde{\omega}^{\Lambda_2}_{l_2m_2\lambda_2\mu_2}(t_0')\tilde{\omega}^{\Lambda_1}_{l_1m_1\lambda_1\mu_1}(t_0) \tag{28}$$

with $\mathcal{Q}_2$ and $\mathcal{Q}_1$ obtained from Eqs. (15) and (16), e.g., $\mathcal{Q}_2=\exp\{i2\pi(m_2n-\mu_2\nu)/N\}$ for $\mathrm{C}N^{\nu}_{n}$ sequences. From Eqs. (27)and (28) follows that the second order average frequency

TABLE I. Expressions for $S^{\square}_{\substack{l_2 m_2 \lambda_2 \mu_2 \\ l_1 m_1 \lambda_1 \mu_1}}$ [Eq. (32)] and $S^{\triangle}_{\substack{l_2 m_2 \lambda_2 \mu_2 \\ l_1 m_1 \lambda_1 \mu_1}}$ [Eq. (35)] provided by the different R/C-categories 1–4 of second order average Hamiltonian terms in the case of RN_n^ν and CN_n^ν sequences. Q_1 and Q_2 are defined as in Eq. (16), e.g., $Q_1 = m_1 n - \mu_1 \nu$ for CN_n^ν sequences and $Q_1 = m_1 n - \mu_1 \nu - \lambda_1 N/2$ for RN_n^ν sequences. The following demonstrates the way to read the selection rules for the first row as an example: $m_1 n - \mu_1 \nu \neq NZ$ for CN_n^ν sequences and $m_1 n - \mu_1 \nu \neq (N/2) Z_{\lambda_1}$ for RN_n^ν sequences.

$S^{\square}_{\substack{l_2 m_2 \lambda_2 \mu_2 \\ l_1 m_1 \lambda_1 \mu_1}}$	$S^{\triangle}_{\substack{l_2 m_2 \lambda_2 \mu_2 \\ l_1 m_1 \lambda_1 \mu_1}}$	Selection rules			C/R category
			CN_n^ν	RN_n^ν	
0	0	$m_1 n - \mu_1 \nu$	$\neq NZ$	$\neq \frac{N}{2} Z_{\lambda_1}$	1
		AND			
		$m_2 n - \mu_2 \nu$	$\neq NZ$	$\neq \frac{N}{2} Z_{\lambda_2}$	
		AND			
		$(m_1 + m_2) n - (\mu_1 + \mu_2) \nu$	$\neq NZ$	$\neq \frac{N}{2} Z_{\lambda_1 + \lambda_2}$	
$-i \frac{\exp\{-i\pi Q_1/N\}}{2N \sin\{\pi Q_1/N\}}$		$m_1 n - \mu_1 \nu$	$\neq NZ$	$\neq \frac{N}{2} Z_{\lambda_1}$	
		AND			
$=$	$\frac{1}{N}$	$m_2 n - \mu_2 \nu$	$\neq NZ$	$\neq \frac{N}{2} Z_{\lambda_2}$	2
		AND			
$i \frac{\exp\{i\pi Q_2/N\}}{2N \sin\{\pi Q_2/N\}}$		$(m_1 + m_2) n - (\mu_1 + \mu_2) \nu$	$= NZ$	$= \frac{N}{2} Z_{\lambda_1 + \lambda_2}$	
		$m_1 n - \mu_1 \nu$	$= NZ$	$= \frac{N}{2} Z_{\lambda_1}$	
		AND			
$-i \frac{\exp\{-i\pi Q_2/N\}}{2N \sin\{\pi Q_2/N\}}$	0	$m_2 n - \mu_2 \nu$	$\neq NZ$	$\neq \frac{N}{2} Z_{\lambda_2}$	3a
		AND			
		$(m_1 + m_2) n - (\mu_1 + \mu_2) \nu$	$\neq NZ$	$\neq \frac{N}{2} Z_{\lambda_1 + \lambda_2}$	
		$m_1 n - \mu_1 \nu$	$\neq NZ$	$\neq \frac{N}{2} Z_{\lambda_1}$	
		AND			
$i \frac{\exp\{-i\pi Q_1/N\}}{2N \sin\{\pi Q_1/N\}}$	0	$m_2 n - \mu_2 \nu$	$= NZ$	$= \frac{N}{2} Z_{\lambda_2}$	3b
		AND			
		$(m_1 + m_2) n - (\mu_1 + \mu_2) \nu$	$\neq NZ$	$\neq \frac{N}{2} Z_{\lambda_1 + \lambda_2}$	
		$m_1 n - \mu_1 \nu$	$= NZ$	$= \frac{N}{2} Z_{\lambda_1}$	
		AND			
$\frac{N-1}{2N}$	$\frac{1}{N}$	$m_2 n - \mu_2 \nu$	$= NZ$	$= \frac{N}{2} Z_{\lambda_2}$	4
		AND			
		$(m_1 + m_2) n - (\mu_1 + \mu_2) \nu$	$= NZ$	$= \frac{N}{2} Z_{\lambda_1 + \lambda_2}$	

term $\overline{\omega}^{\Lambda_2 \times \Lambda_1}_{\substack{l_2 m_2 \lambda_2 \mu_2 \\ l_1 m_1 \lambda_1 \mu_1}}$ may be written

$$\overline{\omega}^{\Lambda_2 \times \Lambda_1}_{\substack{l_2 m_2 \lambda_2 \mu_2 \\ l_1 m_1 \lambda_1 \mu_1}} = \tau_r \kappa_{\substack{l_2 m_2 \lambda_2 \mu_2 \\ l_1 m_1 \lambda_1 \mu_1}} [A^{\Lambda_2}_{l_2 m_2}]^R [A^{\Lambda_1}_{l_1 m_1}]^R \times \exp\{-i(m_2 + m_1)(\alpha^0_{RL} - \omega_r t^0_0)\}. \quad (29)$$

The *dimensionless* second order scaling factor $\kappa_{\substack{l_2 m_2 \lambda_2 \mu_2 \\ l_1 m_1 \lambda_1 \mu_1}}$ may be decomposed into two components,

$$\kappa_{\substack{l_2 m_2 \lambda_2 \mu_2 \\ l_1 m_1 \lambda_1 \mu_1}} = \kappa^{\square}_{\substack{l_2 m_2 \lambda_2 \mu_2 \\ l_1 m_1 \lambda_1 \mu_1}} + \kappa^{\triangle}_{\substack{l_2 m_2 \lambda_2 \mu_2 \\ l_1 m_1 \lambda_1 \mu_1}}, \quad (30)$$

where each contribution, $\kappa^{\square}_{\substack{l_2 m_2 \lambda_2 \mu_2 \\ l_1 m_1 \lambda_1 \mu_1}}$ and $\kappa^{\triangle}_{\substack{l_2 m_2 \lambda_2 \mu_2 \\ l_1 m_1 \lambda_1 \mu_1}}$, results from the integration over rectangular and triangular areas, respectively (Fig. 2). The rectangular part is given by

$$\kappa^{\square}_{\substack{l_2 m_2 \lambda_2 \mu_2 \\ l_1 m_1 \lambda_1 \mu_1}} = \frac{n}{2i} S^{\square}_{\substack{l_2 m_2 \lambda_2 \mu_2 \\ l_1 m_1 \lambda_1 \mu_1}} A^{\square}_{\substack{l_2 m_2 \lambda_2 \mu_2 \\ l_1 m_1 \lambda_1 \mu_1}}, \tag{31}$$

with the sum

$$S^{\square}_{\substack{l_2 m_2 \lambda_2 \mu_2 \\ l_1 m_1 \lambda_1 \mu_1}} = \frac{1}{N^2} \sum_{q'=1}^{N-1} \mathcal{Q}_2^{q'} \sum_{q=0}^{q'-1} \mathcal{Q}_1^{q}. \tag{32}$$

It can be evaluated to the closed expressions shown in Table I and the supplementary material[50] and will be discussed further in the next section. The term $A^{\square}_{\substack{l_2 m_2 \lambda_2 \mu_2 \\ l_1 m_1 \lambda_1 \mu_1}}$ in Eq. (31) corresponds to the product of the *first order* scaling factors of the two interaction Λ_2 and Λ_1 [each calculated from Eq. (23)]:

$$A^{\square}_{\substack{l_2 m_2 \lambda_2 \mu_2 \\ l_1 m_1 \lambda_1 \mu_1}} = \kappa_{l_2 m_2 \lambda_2 \mu_2} \kappa_{l_1 m_1 \lambda_1 \mu_1}. \tag{33}$$

The triangular part in Eq. (30) is given by

$$\kappa^{\triangle}_{\substack{l_2 m_2 \lambda_2 \mu_2 \\ l_1 m_1 \lambda_1 \mu_1}} = \frac{n}{2i} S^{\triangle}_{\substack{l_2 m_2 \lambda_2 \mu_2 \\ l_1 m_1 \lambda_1 \mu_1}} A^{\triangle}_{\substack{l_2 m_2 \lambda_2 \mu_2 \\ l_1 m_1 \lambda_1 \mu_1}} \tag{34}$$

with

$$S^{\triangle}_{\substack{l_2 m_2 \lambda_2 \mu_2 \\ l_1 m_1 \lambda_1 \mu_1}} = \frac{1}{N^2} \sum_{q=0}^{N-1} \mathcal{Q}_2^{q} \mathcal{Q}_1^{q}. \tag{35}$$

This sum may be represented as the closed analytical forms shown in Table I and the supplementary material.[50] Depending on the type of pulse sequence, the term $A^{\triangle}_{\substack{l_2 m_2 \lambda_2 \mu_2 \\ l_1 m_1 \lambda_1 \mu_1}}$ is given by

$$A^{\triangle}_{\substack{l_2 m_2 \lambda_2 \mu_2 \\ l_1 m_1 \lambda_1 \mu_1}} = \begin{cases} d^{l_2}_{m_2 0}(\beta_{RL}) d^{l_1}_{m_1 0}(\beta_{RL}) K_{\substack{m_2 \lambda_2 \mu_2 \\ m_1 \lambda_1 \mu_1}} & \text{for } \mathrm{C}N_n^{\nu}, \\ d^{l_2}_{m_2 0}(\beta_{RL}) d^{l_1}_{m_1 0}(\beta_{RL}) \exp\left\{ -i(\mu_2+\mu_1)\dfrac{\pi \nu}{N} \right\} K_{\substack{m_2 \lambda_2 \mu_2 \\ m_1 \lambda_1 \mu_1}} & \text{for } \mathrm{R}N_n^{\nu} \end{cases} \tag{36}$$

with the factor $K_{\substack{m_2 \lambda_2 \mu_2 \\ m_1 \lambda_1 \mu_1}}$ representing an integral over the basic element $\mathcal{E}^0$, according to

$$\begin{aligned} K_{\substack{m_2 \lambda_2 \mu_2 \\ m_1 \lambda_1 \mu_1}} = \tau_E^{-2} \int_0^{\tau_E} dt^{0\prime} \int_0^{t^{0\prime}} dt^0 \, d^{\lambda_2}_{\mu_2 0}(-\beta^{0\prime}) \\ \times \exp\{ i(\mu_2 \gamma^{0\prime} + m_2 \omega_r t^{0\prime}) \} \\ \times d^{\lambda_1}_{\mu_1 0}(-\beta^0) \exp\{ i(\mu_1 \gamma^0 + m_1 \omega_r t^0) \}. \end{aligned} \tag{37}$$

The calculation of $K_{\substack{m_2 \lambda_2 \mu_2 \\ m_1 \lambda_1 \mu_1}}$ for arbitrary elements $\mathcal{E}^0$ is discussed in the Appendix.

4. Classification of second order average Hamiltonian terms

Different cases have to be distinguished when the sums are evaluated in Eqs. (32) and (35), depending on the exponents in Eq. (16) that dictate *which selection rules are fulfilled*. A second order cross term with pairs of quantum numbers $\{(l_2,m_2,\lambda_2,\mu_2),(l_1,m_1,\lambda_1,\mu_1)\}$ may fall into one of five *R/C categories* denoted 1, 2, 3a, 3b, and 4. Table I summarizes the expressions for the sums $S^{\square}_{\substack{l_2 m_2 \lambda_2 \mu_2 \\ l_1 m_1 \lambda_1 \mu_1}}$ and $S^{\triangle}_{\substack{l_2 m_2 \lambda_2 \mu_2 \\ l_1 m_1 \lambda_1 \mu_1}}$; these are obtained from the generic forms given in the supplementary material.[50]

In case of the R/C-category 1, both sums vanish and the second order term is suppressed: the selection rules are those previously presented in Refs. 11, 12, and 19. In the case of $\mathrm{C}N_n^{\nu}$ sequences they can be transformed to

$$\overline{H}^{\Lambda_2 \times \Lambda_1}_{\substack{l_2 m_2 \lambda_2 \mu_2 \\ l_1 m_1 \lambda_1 \mu_1}} = S^{\square}_{\substack{l_2 m_2 \lambda_2 \mu_2 \\ l_1 m_1 \lambda_1 \mu_1}} = S^{\triangle}_{\substack{l_2 m_2 \lambda_2 \mu_2 \\ l_1 m_1 \lambda_1 \mu_1}} = 0$$

$$\text{if } \begin{cases} m_1 n - \mu_1 \nu \neq NZ \\ \text{AND} \\ m_2 n - \mu_2 \nu \neq NZ \\ \text{AND} \\ (m_2+m_1) n - (\mu_2+\mu_1) \nu \neq NZ \end{cases} \tag{38}$$

where Z is any integer, not necessarily the same for all inequalities. In the case of $\mathrm{R}N_n^{\nu}$ sequences they correspond to

$$\overline{H}^{\Lambda_2 \times \Lambda_1}_{\substack{l_2 m_2 \lambda_2 \mu_2 \\ l_1 m_1 \lambda_1 \mu_1}} = S^{\square}_{\substack{l_2 m_2 \lambda_2 \mu_2 \\ l_1 m_1 \lambda_1 \mu_1}} = S^{\triangle}_{\substack{l_2 m_2 \lambda_2 \mu_2 \\ l_1 m_1 \lambda_1 \mu_1}} = 0$$

$$\text{if } \begin{cases} m_1 n - \mu_1 \nu \neq \frac{N}{2} Z_{\lambda_1} \\ \text{AND} \\ m_2 n - \mu_2 \nu \neq \frac{N}{2} Z_{\lambda_2} \\ \text{AND} \\ (m_2+m_1) n - (\mu_2+\mu_1) \nu \neq \frac{N}{2} Z_{\lambda_2+\lambda_1} \end{cases} \tag{39}$$

where Z_λ represents any integer with the same parity as λ.

If a second order term belongs to one of the R/C-categories 2, 3a, 3b or 4 it is *symmetry allowed* and has to be calculated explicitly. The symmetry-allowed second order terms can be further classified according to the selection rules obeyed for the two involved spin interactions for the corresponding first order average Hamiltonians. In the case of R/C-category 2, *both* terms with the quantum numbers $(l_2,m_2,\lambda_2,\mu_2)$ and $(l_1,m_1,\lambda_1,\mu_1)$ are *suppressed to first order* AHT. Then, both sums, $S^{\square}_{\substack{l_2m_2\lambda_2\mu_2\\ l_1m_1\lambda_1\mu_1}}$ and $S^{\triangle}_{\substack{l_2m_2\lambda_2\mu_2\\ l_1m_1\lambda_1\mu_1}}$, are different from zero and their explicit expressions depend on the spatial and spin quantum numbers, as well as the symmetry numbers of the pulse sequence (see Table I). If a second order term belongs to one of the R/C-categories 3a or 3b, one of the two first order terms, *either* $(l_2,m_2,\lambda_2,\mu_2)$ *or* $(l_1,m_1,\lambda_1,\mu_1)$, is symmetry allowed whereas the other is suppressed. The sum $S^{\triangle}_{\substack{l_2m_2\lambda_2\mu_2\\ l_1m_1\lambda_1\mu_1}}$ vanishes in this case, only leaving the rectangular contribution $S^{\square}_{\substack{l_2m_2\lambda_2\mu_2\\ l_1m_1\lambda_1\mu_1}}$. In case of R/C-category 4, *both* first order terms, $(l_2,m_2,\lambda_2,\mu_2)$ and $(l_1,m_1,\lambda_1,\mu_1)$, are *symmetry allowed* to first order AHT. In general, both sums $S^{\square}_{\substack{l_2m_2\lambda_2\mu_2\\ l_1m_1\lambda_1\mu_1}}$ and $S^{\triangle}_{\substack{l_2m_2\lambda_2\mu_2\\ l_1m_1\lambda_2\mu_1}}$ are nonzero, but their expressions depend neither on the quantum numbers of the terms, nor on the symmetry numbers (n,ν) of the pulse sequence (Table I).

D. Symmetrized second order average Hamiltonian terms

Consider the two second order average Hamiltonian terms $\overline{H}^{\Lambda_2\times\Lambda_1}_{\substack{l_2m_2\lambda_2\mu_2\\ l_1m_1\lambda_1\mu_1}}$ and $\overline{H}^{\Lambda_1\times\Lambda_2}_{\substack{l_1m_1\lambda_1\mu_1\\ l_2m_2\lambda_2\mu_2}}$, related by a simultaneous exchange of the interactions Λ_2 and Λ_1, as well as the *order* of the two sets of quantum numbers $(l_2,m_2,\lambda_2,\mu_2)$ and $(l_1,m_1,\lambda_1,\mu_1)$. Both cross terms are simultaneously symmetry allowed or suppressed and they appear pairwise in the sum of Eq. (25). Therefore, it is convenient to express the second order AH as a sum of *symmetrized* terms according to

$$\overline{H}^{(2)}=\sum_{\substack{\text{interaction}\\ \text{pairs}}}\overline{H}^{(\Lambda_2\times\Lambda_1)}_{\substack{(l_2m_2\lambda_2\mu_2)\\ l_1m_1\lambda_1\mu_1}}, \tag{40}$$

with

$$\overline{H}^{(\Lambda_2\times\Lambda_1)}_{\substack{(l_2m_2\lambda_2\mu_2)\\ l_1m_1\lambda_1\mu_1}}=\overline{H}^{\Lambda_2\times\Lambda_1}_{\substack{l_2m_2\lambda_2\mu_2\\ l_1m_1\lambda_1\mu_1}}+\overline{H}^{\Lambda_1\times\Lambda_2}_{\substack{l_1m_1\lambda_1\mu_1\\ l_2m_1\lambda_2\mu_2}} \tag{41}$$

The terms included in the summation are deduced as follows: First select two interactions Λ_2 and Λ_1 and find the complete set of cross terms recoupled from their *ordered* set $\Lambda_2\times\Lambda_1$ using the selection rules Eqs. (38) or (39). Then form the symmetrized second order AH according to Eq. (41) for *each* of these terms; this procedure automatically takes all cross terms of the set $\Lambda_1\times\Lambda_2$ into account. The protocol is repeated for all *distinct* symmetrized pairs $(\Lambda_2\times\Lambda_1)$.

Equation (26) may now be cast into a symmetrized form

$$\overline{H}^{(\Lambda_2\times\Lambda_1)}_{\substack{(l_2m_2\lambda_2\mu_2)\\ l_1m_1\lambda_1\mu_1}}=\overline{\omega}^{(\Lambda_2\times\Lambda_1)}_{\substack{(l_2m_2\lambda_2\mu_2)\\ l_1m_1\lambda_1\mu_1}}[T^{\Lambda_2}_{\lambda_2\mu_2},T^{\Lambda_1}_{\lambda_1\mu_1}], \tag{42}$$

with the symmetrized cross term interaction frequency given by

$$\overline{\omega}^{(\Lambda_2\times\Lambda_1)}_{\substack{(l_2m_2\lambda_2\mu_2)\\ l_1m_1\lambda_1\mu_1}}=\overline{\omega}^{\Lambda_2\times\Lambda_1}_{\substack{l_2m_2\lambda_2\mu_2\\ l_1m_1\lambda_1\mu_1}}-\overline{\omega}^{\Lambda_1\times\Lambda_2}_{\substack{l_1m_1\lambda_1\mu_1\\ l_2m_2\lambda_2\mu_2}}. \tag{43}$$

By Eq. (29) it may be expressed as

$$\overline{\omega}^{(\Lambda_2\times\Lambda_1)}_{\substack{(l_2m_2\lambda_2\mu_2)\\ l_1m_1\lambda_1\mu_1}}=\tau_r\kappa_{\substack{(l_2m_2\lambda_2\mu_2)\\ l_1m_1\lambda_1\mu_1}}[A^{\Lambda_2}_{l_2m_2}]^R[A^{\Lambda_1}_{l_1m_1}]^R \times\exp\{-i(m_2+m_1)(\alpha^0_{RL}-\omega_r t^0_0)\} \tag{44}$$

with the *symmetrized dimensionless* second order *scaling factor* given by

$$\kappa_{\substack{(l_2m_2\lambda_2\mu_2)\\ l_1m_1\lambda_1\mu_1}}=\kappa_{\substack{l_2m_2\lambda_2\mu_2\\ l_1m_1\lambda_1\mu_1}}-\kappa_{\substack{l_1m_1\lambda_1\mu_1\\ l_2m_2\lambda_2\mu_2}}. \tag{45}$$

E. MQ phase cycles

In this section we discuss the AHT of $\mathcal{S}M^{\chi}$ sequences with $\mathcal{S}=\mathrm{C}N^{\nu}_n$ or $\mathcal{S}=\mathrm{R}N^{\nu}_n$. From the construction of a $\mathcal{S}M^{\chi}$ sequence follows another interaction frame symmetry, in addition to that given in Eq. (17),

$$\tilde{\omega}^{\Lambda}_{lm\lambda\mu}(t_q+pT)=\mathcal{P}^p\tilde{\omega}^{\Lambda}_{lm\lambda\mu}(t_q). \tag{46}$$

Here p is an integer between 0 and $M-1$ and the following substitutions are used:

$$\mathcal{P}=\exp\{i2\pi P/M\}, \tag{47}$$

$$P=-\mu\chi. \tag{48}$$

1. First order average Hamiltonian

The first order average Hamiltonian for an $\mathcal{S}M^{\chi}$ sequence is constructed through Eq. (18), where

$$\overline{\omega}^{\Lambda}_{lm\lambda\mu}=T^{-1}_{\mathrm{SM}}\int_{t^0_0}^{t^0_0+T_{\mathrm{SM}}}dt\,\tilde{\omega}^{\Lambda}_{lm\lambda\mu}(t). \tag{49}$$

From the periodic symmetries Eqs. (17) and (46) this may be simplified to

$$\overline{\omega}^{\Lambda}_{lm\lambda\mu}=\mathrm{S}_{\mu}S_{lm\lambda\mu}\kappa_{lm\lambda\mu}[A^{\Lambda}_{lm}]^R\exp\{-im(\alpha^0_{RL}-\omega_r t^0_0)\} \tag{50}$$

with $S_{lm\lambda\mu}$ and $\kappa_{lm\lambda\mu}$ defined in Eqs. (21) and (23), respectively, and the sum S_{μ} stemming from the MQ phase cycle:

$$\mathrm{S}_{\mu}=\frac{1}{M}\sum_{p=0}^{M-1}\mathcal{P}^p=\begin{cases}0 & \text{if } \mathcal{P}\neq 1\Leftrightarrow P\neq MZ,\\ 1 & \text{if } \mathcal{P}=1\Leftrightarrow P=MZ.\end{cases} \tag{51}$$

The product of sums $\mathrm{S}_{\mu}S_{lm\lambda\mu}$ gives rise to the selection rules for the first order AH terms of an $\mathcal{S}M^{\chi}$ sequence,[35]

$$\overline{H}^{\Lambda}_{lm\lambda\mu}=\mathbb{S}_{\mu}S_{lm\lambda\mu}=0 \quad \text{if}\begin{cases}(mn-\mu\nu\neq NZ) & \text{OR } (\mu\chi\neq MZ') \quad \text{for } (\mathrm{C}N_n^{\nu})M^{\chi},\\ \left(mn-\mu\nu\neq\dfrac{N}{2}Z_{\lambda}\right) & \text{OR } (\mu\chi\neq MZ') \quad \text{for } (\mathrm{R}N_n^{\nu})M^{\chi},\end{cases} \tag{52}$$

where Z and Z' are arbitrary integers and Z_{λ} is any integer with the same parity as λ. As discussed in Refs. 13 and 35 the first order selection rule for the AH of a $\mathcal{SM}^{\chi}$ scheme is related to that of $\mathrm{C}N_n^{\nu}$ and $\mathrm{R}N_n^{\nu}$ sequences [Eq. (22)], with the *additional requirement* that all second order terms are *suppressed* if the product $\mu\chi$ is *not* an integer multiple of M.

2. Second order average Hamiltonian

The second order average Hamiltonian for an $\mathcal{SM}^{\chi}$ sequence is given by Eq. (26), with the time integration extending over the entire supercycle

$$\overline{\omega}^{\Lambda_2\times\Lambda_1}_{\substack{l_2m_2\lambda_2\mu_2\\ l_1m_1\lambda_1\mu_1}}=(2iT_{\mathrm{SM}})^{-1}\int_{t_0^0}^{t_0^0+T_{\mathrm{SM}}}dt'\int_{t_0^0}^{t'}dt \times\tilde{\omega}^{\Lambda_2}_{l_2m_2\lambda_2\mu_2}(t')\tilde{\omega}^{\Lambda_1}_{l_1m_1\lambda_1\mu_1}(t). \tag{53}$$

In the presence of an $\mathcal{SM}^{\chi}$ sequence, the interaction frame symmetry of $\tilde{\omega}^{\Lambda_2}_{l_2m_2\lambda_2\mu_2}$ implies the following property of a product of two such terms:

$$\tilde{\omega}^{\Lambda_2}_{l_2m_2\lambda_2\mu_2}(t_{q'}+p'T)\tilde{\omega}^{\Lambda_1}_{l_1m_1\lambda_1\mu_1}(t_q+pT) =\mathcal{P}_2^{p'}\mathcal{P}_1^{p}\tilde{\omega}^{\Lambda_2}_{l_2m_2\lambda_2\mu_2}(t_{q'})\tilde{\omega}^{\Lambda_1}_{l_1m_1\lambda_1\mu_1}(t_q) \tag{54}$$

with $\mathcal{P}_1=\exp\{-i2\pi\mu_1\chi/M\}$ and $\mathcal{P}_2=\exp\{-i2\pi\mu_2\chi/M\}$ given from Eqs. (47) and (48). The term $\overline{\omega}^{\Lambda_2\times\Lambda_1}_{\substack{l_2m_2\lambda_2\mu_2\\ l_1m_1\lambda_1\mu_1}}$ may consequently be expressed as

$$\overline{\omega}^{\Lambda_2\times\Lambda_1}_{\substack{l_2m_2\lambda_2\mu_2\\ l_1m_1\lambda_1\mu_1}}=\tau_r\kappa^{\mathrm{SM}}_{\substack{l_2m_2\lambda_2\mu_2\\ l_1m_1\lambda_1\mu_1}}[A^{\Lambda_2}_{l_2m_2}]^R[A^{\Lambda_1}_{l_1m_1}]^R \times\exp\{-i(m_2+m_1)(\alpha^0_{RL}-\omega_r t_0^0)\}, \tag{55}$$

where $\kappa^{\mathrm{SM}}_{\substack{l_2m_2\lambda_2\mu_2\\ l_1m_1\lambda_1\mu_1}}$ is the dimensionless second order scaling factor of the $\mathcal{SM}^{\chi}$ sequence. In analogy with Eq. (30) it may be written as a sum of two components,

$$\kappa^{\mathrm{SM}}_{\substack{l_2m_2\lambda_2\mu_2\\ l_1m_1\lambda_1\mu_1}}=\kappa^{\mathrm{SM}\square}_{\substack{l_2m_2\lambda_2\mu_2\\ l_1m_1\lambda_1\mu_1}}+\kappa^{\mathrm{SM}\triangle}_{\substack{l_2m_2\lambda_2\mu_2\\ l_1m_1\lambda_1\mu_1}}. \tag{56}$$

The rectangular part is given by

$$\kappa^{\mathrm{SM}\square}_{\substack{l_2m_2\lambda_2\mu_2\\ l_1m_1\lambda_1\mu_1}}=\frac{Mn}{2i}\mathbb{S}^{\square}_{\mu_2\mu_1}S_{l_2m_2\lambda_2\mu_2}S_{l_1m_1\lambda_1\mu_1} \times\kappa_{l_2m_2\lambda_2\mu_2}\kappa_{l_1m_1\lambda_1\mu_1}, \tag{57}$$

where the sums $S_{l_2m_2\lambda_2\mu_2}$ and $S_{l_1m_1\lambda_1\mu_1}$ are defined by Eq. (21) with $\kappa_{l_2m_2\lambda_2\mu_2}$ and $\kappa_{l_1m_1\lambda_1\mu_1}$ being the corresponding first order scaling factors and the sum $\mathbb{S}^{\square}_{\mu_2\mu_1}$ corresponding to

$$\mathbb{S}^{\square}_{\mu_2\mu_1}=\frac{1}{M^2}\sum_{p'=1}^{M-1}\mathcal{P}_2^{p'}\sum_{p=0}^{p'-1}\mathcal{P}_1^{p}. \tag{58}$$

It may be simplified to the closed analytical forms given in Table II, obtained from the generic form given in the supplementary material.[50] The triangular part in Eq. (56) is given by

$$\kappa^{\mathrm{SM}\triangle}_{\substack{l_2m_2\lambda_2\mu_2\\ l_1m_1\lambda_1\mu_1}}=M\mathbb{S}^{\triangle}_{\mu_2\mu_1}\kappa_{\substack{l_2m_2\lambda_2\mu_2\\ l_1m_1\lambda_1\mu_1}}, \tag{59}$$

TABLE II. Expressions for $\mathbb{S}^{\square}_{\mu_2\mu_1}$ [Eq. (58)] and $\mathbb{S}^{\triangle}_{\mu_2\mu_1}$ [Eq. (60)] depending on the MQ-category of the second order average Hamiltonian term for MQ-phase cycles $\mathcal{SM}^{\chi}$.

$\mathbb{S}^{\square}_{\mu_2\mu_1}$	$\mathbb{S}^{\triangle}_{\mu_2\mu_1}$	MQ selection rules	MQ category
0	0	$\mu_1\chi\neq MZ$ AND $\mu_2\chi\neq MZ$ AND $(\mu_1+\mu_2)\chi\neq MZ$	1
$i\dfrac{\exp\{i\pi\mu_1\chi/M\}}{2M\sin\{\pi\mu_1\chi/M\}}$ = $-i\dfrac{\exp\{-i\pi\mu_2\chi/M\}}{2M\sin\{\pi\mu_2\chi/M\}}$	$\dfrac{1}{M}$	$\mu_1\chi\neq MZ$ AND $\mu_2\chi\neq MZ$ AND $(\mu_1+\mu_2)\chi=MZ$	2
$i\dfrac{\exp\{i\pi\mu_2\chi/M\}}{2M\sin\{\pi\mu_2\chi/M\}}$	0	$\mu_1\chi=MZ$ AND $\mu_2\chi\neq MZ$ AND $(\mu_1+\mu_2)\chi\neq MZ$	3a
$-i\dfrac{\exp\{i\pi\mu_1\chi/M\}}{2M\sin\{\pi\mu_1\chi/M\}}$	0	$\mu_1\chi\neq MZ$ AND $\mu_2\chi=MZ$ AND $(\mu_1+\mu_2)\chi\neq MZ$	3b
$\dfrac{M-1}{2M}$	$\dfrac{1}{M}$	$\mu_1\chi=MZ$ AND $\mu_2\chi=MZ$ AND $(\mu_1+\mu_2)\chi=MZ$	4

where $\kappa_{\substack{l_2m_2\lambda_2\mu_2\\ l_1m_1\lambda_1\mu_1}}$ is the second order scaling factor defined in Eq. (30) and the sum $\mathbb{S}^{\triangle}_{\mu_2\mu_1}$ defined by

$$\mathbb{S}^{\triangle}_{\mu_2\mu_1}=\frac{1}{M^2}\sum_{p=0}^{M-1}\mathcal{P}_2^p\mathcal{P}_1^p. \tag{60}$$

Its simplified analytical forms are given in Table II.

Similarly to the previous treatment of the sums $S^{\square}_{\substack{l_2m_2\lambda_2\mu_2\\ l_1m_1\lambda_1\mu_1}}$ and $S^{\triangle}_{\substack{l_2m_2\lambda_2\mu_2\\ l_1m_1\lambda_1\mu_1}}$ in the case of CN_n^ν or RN_n^ν sequences, five different *MQ categories* must be distinguished when evaluating $\mathbb{S}^{\square}_{\mu_2\mu_1}$ and $\mathbb{S}^{\triangle}_{\mu_2\mu_1}$ for an $\mathcal{S}M^\chi$ sequence. As these five categories couple together with the five categories provided by the compound CN_n^ν or RN_n^ν schemes, altogether 25 different cases (presented in the supplementary material[50]) have to be distinguished when analyzing the second order average Hamiltonian of an $\mathcal{S}M^\chi$ sequence.

3. Second order selection rules for $\mathcal{S}M^\chi$ sequences

From the definition of the scaling factors for the second order average Hamiltonian terms in the presence of a $\mathcal{S}M^\chi$ sequence, the selection rules for the second order terms can be expressed as

$$\overline{H}^{\Lambda_2\times\Lambda_1}_{\substack{l_2m_2\lambda_2\mu_2\\ l_1m_1\lambda_1\mu_1}}=0$$

$$\text{if}\ \begin{cases}(\mathbb{S}^{\triangle}_{\mu_2\mu_1}=0 \quad \text{OR}\ \ S^{\square}_{\substack{l_2m_2\lambda_2\mu_2\\ l_1m_1\lambda_1\mu_1}}=0)\\ \text{AND}\\ (\mathbb{S}^{\square}_{\mu_2\mu_1}=0 \quad \text{OR}\ \ S_{l_2m_2\lambda_2\mu_2}=0 \quad \text{OR}\ \ S_{l_1m_1\lambda_1\mu_1}=0).\end{cases} \tag{61}$$

This condition may be expressed in terms of the spin and spatial quantum numbers of the cross term and the symmetry numbers of the $\mathcal{S}M^\chi$ scheme,[35]

$$\overline{H}^{\Lambda_2\times\Lambda_1}_{\substack{l_2m_2\lambda_2\mu_2\\ l_1m_1\lambda_1\mu_1}}=0 \quad \text{if}\ (A\ \ \text{AND}\ \ B). \tag{62}$$

For $(RN_n^\nu)M^\chi$ sequences, the logical expressions A and B (which may evaluate either to "true" or "false") are given by

$$A=\left(\begin{array}{c} m_1n-\mu_1\nu\neq\dfrac{N}{2}Z_{\lambda_1}\\ \text{AND}\\ m_2n-\mu_2\nu\neq\dfrac{N}{2}Z_{\lambda_2}\\ \text{AND}\\ (m_2+m_1)n-(\mu_2+\mu_1)\nu\neq\dfrac{N}{2}Z_{\lambda_2+\lambda_1}\end{array}\right)$$
$$\text{OR}\ \ (\mu_1+\mu_2)\chi\neq MZ \tag{63}$$

and

$$B=\left(\begin{array}{c} m_1n-\mu_1\nu\neq\dfrac{N}{2}Z_{\lambda_1}\\ \text{OR}\\ m_2n-\mu_2\nu\neq\dfrac{N}{2}Z_{\lambda_2}\end{array}\right)\ \text{OR}\ \left(\begin{array}{c}\mu_1\chi\neq MZ\\ \text{AND}\\ \mu_2\chi\neq MZ\\ \text{AND}\\ (\mu_1+\mu_2)\chi\neq MZ\end{array}\right). \tag{64}$$

The corresponding inequalities for $(CN_n^\nu)M^\chi$ schemes are obtained by the substitution $(N/2)Z_\lambda\rightarrow NZ'$. If Eq. (62) is not fulfilled, the second order average Hamiltonian term is recoupled due to the combined C/R and MQ phase-cycle symmetries.

Condition A is the direct second order analogue of the first order selection rule Eq. (52): the role of MQ phase cycling is simply to impose the requirement that for $\chi=\pm1$, the sum of spin components $(\mu_2+\mu_1)$ of the recoupled cross term must be an integer multiple of M. However, due to the presence of term B, it is *not necessarily* true that all cross terms recoupled by an $\mathcal{S}M^\chi$ sequence satisfy $(\mu_1+\mu_2)\chi=MZ$. Equation (64) implies that a cross term is *also* symmetry allowed if both its components, $(l_2,m_2,\lambda_2,\mu_2)$ and $(l_1,m_1,\lambda_1,\mu_1)$, are *simultaneously* recoupled to first order, and *additionally*, at least one of them has a spin component being an integer multiple of M [or that the sum $(\mu_1+\mu_2)$ fulfill this requirement]. However, for most symmetries (N,n,ν), contributions from Eq. (64) are rare.

F. The phase inversion supercycle

In this work, our primary concern is the combination of MQ phase cycles $\mathcal{S}M^\chi$ [Fig. 1(d)] and phase inversion supercycles $\mathcal{S}\mathcal{S}'$ [Fig. 1(e)], as they may provide 3Q selective recoupling. However, as a complete theoretical account of $(\mathcal{S}\mathcal{S}')M^\chi$ schemes is out of the scope of this paper, we will only briefly discuss the most import results.

A phase inversion supercycle modifies the first order AH terms [Eq. (18)] recoupled by a sequence $\mathcal{S}$ in the following way:[13,23]

$$\overline{H}^{\Lambda}_{lm\lambda\mu}=\tfrac{1}{2}(\overline{\omega}^{\Lambda}_{lm\lambda\mu}+(-1)^\mu(\overline{\omega}^{\Lambda}_{lm\lambda\mu})^*)T^{\Lambda}_{\lambda\mu}. \tag{65}$$

The frequency $\overline{\omega}^{\Lambda}_{lm\lambda\mu}$ is given by Eq. (20); upon the supercycling procedure $\mathcal{S}\rightarrow\mathcal{S}\mathcal{S}'$, it is replaced by its real or imaginary part, depending on the value of μ. Generally, it follows that the resulting first order scaling factor for the recoupled interaction of the supercycle $\mathcal{S}\mathcal{S}'$ is smaller than that of the sequence $\mathcal{S}$, and that the first order AH is not γ-encoded.[13,23]

A similar effect occurs in the second order AH: under the assumption that *both* components of a cross term $\{(l_2,m_2,\lambda_2,\mu_2),(l_1,m_1,\lambda_1,\mu_1)\}$ are *not simultaneously recoupled to first order,* i.e., if the cross term falls into one of the R/C-categories 2, 3a, and 3b, the second order AH terms in Eq. (26) of the supercycle $\mathcal{S}\mathcal{S}'$ are given by[51,52]

$$\overline{H}^{\Lambda_2\times\Lambda_1}_{\substack{l_2m_2\lambda_2\mu_2\\ l_1m_1\lambda_1\mu_1}}=\frac{1}{2}(\overline{\omega}^{\Lambda_2\times\Lambda_1}_{\substack{l_2m_2\lambda_2\mu_2\\ l_1m_1\lambda_1\mu_1}}-(-1)^{\mu_2+\mu_1}(\overline{\omega}^{\Lambda_2\times\Lambda_1}_{\substack{l_2m_2\lambda_2\mu_2\\ l_1m_1\lambda_1\mu_1}})^*)$$
$$\times[T^{\Lambda_2}_{\lambda_2\mu_2},T^{\Lambda_1}_{\lambda_1\mu_1}], \tag{66}$$

TABLE III. The number of recoupled first and second order dipolar AH terms for various pulse sequences $\mathcal{S}$. $\mathcal{N}$ represent term counts *per coupling* in the case of $\bar{H}^{(1)}$, whereas those for $\bar{H}^{(2)}$ are for *one pair* of dipolar couplings. Note that $R18_3^7$ is inherently 3Q/ZQ selective, i.e., $\mathcal{N}_{1Q}=\mathcal{N}_{2Q}=0$ up to second order, whereas the other schemes are not. However, their corresponding 3Q phase cycles $\mathcal{S}M^x$ are 3Q/ZQ selective. The sequences suppress all other interactions to first order, except J couplings. In the case of $C7_2^{-1}$, isotropic chemical shifts are also recoupled.

$\mathcal{S}$	Class	$\mathcal{N}_{ZQ}[\bar{H}^{(1)}]$	$\mathcal{N}_{1Q}[\bar{H}^{(1)}]$	$\mathcal{N}_{2Q}[\bar{H}^{(1)}]$	$\mathcal{N}_{ZQ}[\bar{H}^{(2)}]$	$\mathcal{N}_{1Q}[\bar{H}^{(2)}]$	$\mathcal{N}_{2Q}[\bar{H}^{(2)}]$	$\mathcal{N}_{3Q}[\bar{H}^{(2)}]$	$\mathcal{N}^{(+3)}$	$\mathcal{T}^{(+3)}$ and C/R categories
$R14_3^2$	I	0	0	0	20	8	0	4	1	2: {(2, 1, 2, 2), (2, 1, 2, 1)}
$R18_3^7$	I	0	0	0	20	0	0	8	2	2: {(2, −1, 2, 2), (2, 2, 2, 1)} 2: {(2, 2, 2, 2), (2, −1, 2, 1)}
$C7_2^{-1}$	II	0	0	2	32	40	28	20	5	3b: {(2, −1, 2, 2), (2, −2, 2, 1)} 3b: {(2, −1, 2, 2), (2, −1, 2, 1)} 3b: {(2, −1, 2, 2), (2, 1, 2, 1)} 3b: {(2, −1, 2, 2), (2, 2, 2, 1)} 2: {(2, 1, 2, 2), (2, 1, 2, 1)}
$R8_1^{-1}$	III	0	2	2	44	56	34	32	8	3b: {(2, −2, 2, 2), (2, −2, 2, 1)} 3b: {(2, −2, 2, 2), (2, 1, 2, 1)} 3b: {(2, −2, 2, 2), (2, 2, 2, 1)} 2: {(2, −1, 2, 2), (2, −2, 2, 1)} 4: {(2, −2, 2, 2), (2, −1, 2, 1)} 3a: {(2, −1, 2, 2), (2, −1, 2, 1)} 3a: {(2, 1, 2, 2), (2, −1, 2, 1)} 3a: {(2, 2, 2, 2), (2, −1, 2, 1)}

where $\bar{\omega}^{\Lambda_2\times\Lambda_1}_{\substack{l_2m_2\lambda_2\mu_2\\ l_1m_1\lambda_1\mu_1}}$ is given by Eq. (29). Hence, upon phase inversion supercycling, the frequency $\bar{\omega}^{\Lambda_2\times\Lambda_1}_{\substack{l_2m_2\lambda_2\mu_2\\ l_1m_1\lambda_1\mu_1}}$ is replaced by its real or imaginary part depending on the value of $\mu_2+\mu_1$. It may be concluded from Eq. (66) that $\bar{H}^{\Lambda_2\times\Lambda_1}_{\substack{l_2m_2\lambda_2\mu_2\\ l_1m_1\lambda_1\mu_1}}$ vanishes over the sequence $\mathcal{S}\mathcal{S}'$ if the following three conditions are simultaneously obeyed: (i) the term belongs to the R/C-category 2, (ii) $l_2=l_1$ and $\lambda_2=\lambda_1$, and (iii) $\mu_2+\mu_1=0$. Therefore, all ZQ terms of category 2 vanish upon phase inversion supercycling. This property is exploited below to convert 3Q/ZQ-selective sequences into 3Q-selective ones. The two $(\mathcal{S}\mathcal{S}')M^x$ schemes generated from Eqs. (4) and (5) provide identical second order average Hamiltonians under these conditions.

IV. FEATURES OF 3Q RECOUPLING

A. Average Hamiltonian

Here we assume a system of N_S coupled spins-1/2 $(i,j,k,\ldots)$ and apply the previously introduced second order AHT to the case of 3Q recoupling. A 3Q term may appear in the second order average Hamiltonian as a cross term between a double-quantum operator associated with one dipolar coupling and another single-quantum operator of a *different* coupling, according to the commutators

$$[T^{ij}_{2\pm2},T^{ik}_{2\pm1}]=-[T^{ij}_{2\pm1},T^{ik}_{2\pm2}]$$

$$=\mp\frac{1}{\sqrt{2}}T^{ijk}_{3\pm3}=\frac{1}{4}S_i^{\pm}S_j^{\pm}S_k^{\pm}. \tag{67}$$

The second order average Hamiltonian of a sequence $\mathcal{S}$ then comprises terms of the form $\{\Lambda_2\times\Lambda_1;(l_2,m_2,\lambda_2,\mu_2),(l_1,m_1,\lambda_1,\mu_1)\}$, with

$$\{ij\times ik;(2,m_2,2,\pm2),(2,m_1,2,\pm1)\},$$

$$\{ij\times ik;(2,m_1,2,\pm1),(2,m_2,2,\pm2)\}.$$

In this section, we explicitly indicate the order of couplings within each cross term. Assume the sequence recouples in total $\mathcal{N}_{3Q}$ such terms for *each* ordered set of dipolar pairs $ij\times ik$. The number $\mathcal{N}_{3Q}$ is always a multiple of 4 (cf. Table III): from the selection rules follow that for each +3Q term $\{ij\times ik;(2,m_2,2,2),(2,m_1,2,1)\}$ (involving the commutator $[T^{ij}_{22},T^{ik}_{21}]$), simultaneous recoupling occurs of the +3Q term $\{ij\times ik;(2,m_1,2,1),(2,m_2,2,2)\}$ (involving $[T^{ij}_{21},T^{ik}_{22}]$). Also, the two corresponding −3Q terms $\{ij\times ik;(2,-m_2,2,-2),(2,-m_1,2,-1)\}$ and $\{ij\times ik;(2,-m_1,2,-1),(2,-m_2,2,-2)\}$ are recoupled. An identical set of $\mathcal{N}_{3Q}$ cross terms is recoupled for the pair $ik\times ij$.

Onwards, we focus on the *symmetrized* cross terms $\{(ij\times ik);(2,m_2,2,\pm2),(2,m_1,2,\pm1)\}$ that includes *both* $ij\times ik$ and $ik\times ij$ contributions. Hence, there are $\mathcal{N}_{3Q}$ symmetrized terms to consider for each symmetrized pair of couplings. For a system of N_S spins, there are $N_S(N_S-1)/2$ distinct dipolar couplings. There are $N_S(N_S-1)(N_S-2)/2$ *symmetrized pairs* of couplings $(ij\times ik)$ that may produce ±3Q operators, and a total of $\mathcal{N}_{3Q}N_S(N_S-1)(N_S-2)/2$ distinct $\bar{\omega}^{(\Lambda_2\times\Lambda_1)}_{(\substack{l_2m_2\lambda_2\mu_2\\ l_1m_1\lambda_1\mu_1})}$ contributions to the second order average Hamiltonian. For example, in a three-spin system, there are $3\mathcal{N}_{3Q}$ distinct symmetrized terms.

In the following, we focus on a *subset* of $\mathcal{N}^{(+3)}+3Q$ terms recoupled by a given pulse sequence $\mathcal{S}$ and originating from *one pair* $(ij\times ik)$. This set is denoted $\mathcal{T}^{(+3)}=\{\mathcal{T}_1,\mathcal{T}_2,\ldots,\mathcal{T}_{\mathcal{N}^{(+3)}}\}$, where each element $\mathcal{T}_r$ represents the net contribution from the cross term conforming to $\{(ij\times ik);(2,m_2,2,2),(2,m_1,2,1)\}$ and that obtained after ex-

changing the order of the sets of quantum numbers: $\{(ij\times ik);(2,m_1,2,1),(2,m_2,2,2)\}$. Expressed in terms of symmetrized Hamiltonians, the contribution from $\mathcal{T}_r$ amounts to

$$\bar{H}^{(ij\times ik)}_{\mathcal{T}_r}=\bar{H}^{(ij\times ik)}_{\binom{2m_2 22}{2m_1 21}}+\bar{H}^{(ij\times ik)}_{\binom{2m_1 21}{2m_2 22}} \tag{68}$$

with each term given by a sum according to Eq. (41). The various elements $\mathcal{T}_r$ only differ in the combinations of (m_2,m_1), and each of them comprise four parts: two contributions from the symmetrization procedure, and two originating from only exchanging the order of the sets of quantum numbers while the order of interactions $ij\times ik$ is kept,

$$\left\{\begin{array}{l}\{ij\times ik;(2,m_2,2,2),(2,m_1,2,1)\},\{ik\times ij;(2,m_2,2,2),(2,m_1,2,1)\},\\ \{ij\times ik;(2,m_1,2,1),(2,m_2,2,2)\},\{ik\times ij;(2,m_1,2,1),(2,m_2,2,2)\}\end{array}\right\}.$$

The total second order $+3$Q part of the average Hamiltonian is the sum over all terms within $\mathcal{T}^{(+3)}$ and all symmetrized pairs of dipolar couplings:

$$\bar{H}^{(2)}_{+3\mathrm{Q}}=\sum_{ij,ik}\sum_{r=1}^{\mathcal{N}^{(+3)}}\bar{H}^{(ij\times ik)}_{\mathcal{T}_r}. \tag{69}$$

By combining Eq. (68) with the commutator relationships Eq. (67) we get

$$\begin{aligned}\bar{H}^{(ij\times ik)}_{\mathcal{T}_r}&=\frac{1}{4}\bar{\omega}^{(ij\times ik)}_{\mathcal{T}_r}S_i^+S_j^+S_k^+\\&=\frac{1}{4}\{\bar{\omega}^{(ij\times ik)}_{\binom{2m_2 22}{2m_1 21}}-\bar{\omega}^{(ij\times ik)}_{\binom{2m_1 21}{2m_2 22}}\}S_i^+S_j^+S_k^+.\end{aligned} \tag{70}$$

In the case of a $\mathcal{S}3^{\pm 1}$ phase cycle, each symmetrized term $\bar{\omega}^{(ij\times ik)}_{\binom{2m_2 22}{2m_1 21}}$ is calculated from Eq. (43), whereas for nested 3Q phase-inversion supercycles $(\mathcal{SS}')3^{\pm 1}$ the calculation proceeds through Eq. (66). Expressions for the frequencies $\bar{\omega}^{(ij\times ik)}_{\mathcal{T}_r}$ are given in the supplementary material.[50] The total 3Q AH may be calculated from

$$\bar{H}^{(2)}_{3\mathrm{Q}}=\bar{H}^{(2)}_{+3\mathrm{Q}}+\bar{H}^{(2)}_{-3\mathrm{Q}} \tag{71}$$

with $\bar{H}^{(2)}_{-3\mathrm{Q}}=\{\bar{H}^{(2)}_{+3\mathrm{Q}}\}^\dagger$. From this follows that it is unnecessary to explicitly consider the set of -3Q terms (i.e., $\mathcal{T}^{(-3)}$). Note, however, that for 3Q/ZQ-selective sequences, it is necessary to also include the second order ZQ average Hamiltonian ($\bar{H}^{(2)}_{\mathrm{ZQ}}$), constructed analogously to $\bar{H}^{(2)}_{3\mathrm{Q}}$, and consider the total Hamiltonian

$$\bar{H}^{(2)}=\bar{H}^{(2)}_{3\mathrm{Q}}+\bar{H}^{(2)}_{\mathrm{ZQ}}. \tag{72}$$

B. 3QC excitation

A 3Q-selective Hamiltonian of the form Eq. (71) effects 3QC excitation in multispin systems by conversion of longitudinal equilibrium magnetization ($S_z=S_{iz}+S_{jz}\cdots$) directly into 3QC. The excitation dynamics is particularly simple in a three-spin system as it is confined to a subspace spanned by the two states $|\alpha\alpha\alpha\rangle$ and $|\beta\beta\beta\rangle$, and may be described within the fictitious spin-1/2 formalism.[53,54] We omit the details, as Ref. 6 outlines the general idea of exciting $(\pm M)$QC by the action of an Hamiltonian comprising only $(\pm M)$Q operators on equilibrium magnetization from M spins, and detailed treatments of 2QC excitation in a spin pair may be found in Refs. 55 and 56. The 3QF efficiency is defined as the amplitude obtained after the coherence transfer process $S_z\rightarrow 3\mathrm{QC}\rightarrow S_z$, and is formally given by

$$E_{3\mathrm{Q}}=\mathrm{Tr}\{S_zU_{\mathrm{rec}}(\hat{P}_{3\mathrm{Q}}U_{\mathrm{exc}}S_zU_{\mathrm{exc}}^\dagger)U_{\mathrm{rec}}^\dagger\}/\mathrm{Tr}\{S_z^2\}, \tag{73}$$

where $\hat{P}_{3\mathrm{Q}}$ is a 3QC projection superoperator. U_{exc} and U_{rec} represent the propagators used for 3QC excitation and reconversion, respectively. They are related through $U_{\mathrm{rec}}=R_z(\Phi_{\mathrm{rec}})U_{\mathrm{exc}}R_z(\Phi_{\mathrm{rec}})^\dagger$, with Φ_{rec} being the phase shift applied to the reconversion pulses [see Fig. 1(g)].

Assuming a 3Q Hamiltonian [Eq. (71)] of *three* coupled spins, the 3QF efficiency may be calculated analytically for a single crystallite orientation Ω_{MR} according to

$$\begin{aligned}&E_{3\mathrm{Q}}(\tau_{\mathrm{exc}})\\&=-\frac{3}{4}\sin^2\left\{\frac{1}{2}\left|\sum_{ij,ik}\sum_{r=1}^{\mathcal{N}^{(+3)}}\bar{\omega}^{(ij\times ik)}_{\mathcal{T}_r}\right|\tau_{\mathrm{exc}}\right\}\cos\{3\Phi_{\mathrm{rec}}\}.\end{aligned} \tag{74}$$

Hence, the optimal efficiency of 3/4 is obtained[57] when Φ_{rec} equals any integer multiple of $\pi/3$ (including zero). The maximum theoretical 3QF efficiency in an isotropic powder amounts to $\approx$55%. However, not all 3Q-selective pulse sequences attain this limit due to other orientational aspects of the 3Q Hamiltonian; a detailed discussion is out of the scope of the present paper and will be given elsewhere.

C. Classification of 3Q recoupling sequences

Almost all $\mathrm{C}N_n^\nu$ and $\mathrm{R}N_n^\nu$ sequences give 3Q-recoupling, implying that the corresponding $(\mathrm{R}N_n^\nu)3^1$ and $(\mathrm{C}N_n^\nu)3^1$ MQ phase-cycles effect 3Q/ZQ-selective recoupling. However, additional criteria must be used in the search for practically feasible 3Q recoupling sequences. Here we examine useful classifications of symmetry-based pulse schemes that assists this search and helps predicting the properties of second order 3Q recoupling sequences. It is important to note that the task of MQ phase cycling is to suppress the largest possible number of undesired MQ order terms in the AH generated by the sequence $\mathcal{S}$, while the scaling factors of its 3Q terms remain, in general, unchanged. This implies that the properties of the resulting MQ phase cycle may be assessed from the properties of the compound sequence $\mathcal{S}$.

We have classified the second order *cross terms* in five categories depending on the subset of inequalities in Eqs. (38) and (39) that are obeyed by their sets of quantum numbers. Here we discuss an *additional classification* of the 3Q *recoupling sequences*[35] and examine the relationship between the two classifications. The desired 3Q terms, $\{(2,m_2,2,\pm 2),(2,m_1,2,\pm 1)\}$ arise in second order AHT as cross terms between a 2Q term and a 1Q term, each of which may be recoupled OR decoupled to first order. We therefore dub $\mathcal{S}$ as a ''class I,'' ''class II'' or ''class III'' sequence, depending on whether *neither, one, or both* terms conforming to $(2,m_2,2,\pm 2)$ and $(2,m_1,2,\pm 1)$ *are recoupled to first* order, respectively.

In the case of class I sequences, we demand that all homonuclear dipolar terms (including ZQ terms) are suppressed to first order; they correspond to (first order) homonuclear *decoupling* sequences. Class I sequences have the most restrictive selection rules, and therefore recouple the smallest number of second order 3Q and ZQ terms, *all* of which belong to R/C-category 2. There is an important subset of class I sequences that provide 3Q/ZQ-selective recoupling by the *sequence* $\mathcal{S}$ *itself*, i.e., all 1Q and 2Q terms are suppressed up to second order AHT. This applies, for example, to $C15_1^5$, $C15_2^5$, $C9_3^4$, and all $R18_3^\nu$ sequences. Class II sequences provide *either* 1Q *or* 2Q dipolar recoupling to first order AHT. A recoupled 3Q cross term may belong to one of the R/C-categories 2, 3a or 3b, but not to category 4. Note that there is no restriction on the ZQ AH, as terms of the form $\{(l,m,\lambda,\mu),(l,-m,\lambda,-\mu)\}$ are in general recoupled, and they may conform to any R/C-categories 2–4. Class III sequences recouple both 1Q *and* 2Q dipolar terms to first order. In the case of $(RN_n^\nu)3^{\pm 1}$ sequences, the recoupled terms obey the full selection rule of Eq. (62), and each element in both sets of recoupled 3Q and ZQ terms may conform to any of the R/C-categories 2–4.

Examples of some pulse sequences are listed in Table III. The total number of 3Q terms recoupled by a given $\mathcal{S}3^{\pm 1}$ sequence increases as the selection rules relax. However, class I sequences are advantageous because they most efficiently suppress 1Q and 2Q terms (which interfere with the 3Q recoupling). As no dipolar terms are recoupled to first order by class I 3Q-phase cycles $\mathcal{S}3^{\pm 1}$, they preclude recoupling of second order ZQ terms of R/C-categories 3a, 3b, and 4: from Sec. III follows that 3Q-*selective recoupling is achieved by all* $(\mathcal{S}\mathcal{S}')3^{\pm 1}$ *schemes if* $\mathcal{S}$ *belongs to class* I.

V. DESIGN PRINCIPLES OF 3Q RECOUPLING SEQUENCES

A. Numerical simulation strategies

To assess the performance of 3Q recoupling sequences, we performed a variety of numerical simulations. These refer to calculated 3QF efficiency curves from $\mathcal{S}3^1$ and $(\mathcal{S}\mathcal{S}')3^1$ pulse schemes assuming a three-spin system in a powder, with dipolar couplings representative for $^{13}C_3$–alanine and chemical shift interactions included when noted. All simulations represent powder averages from 538 crystallite orientations selected by the ZCW scheme[58–60] and were carried out as follows:

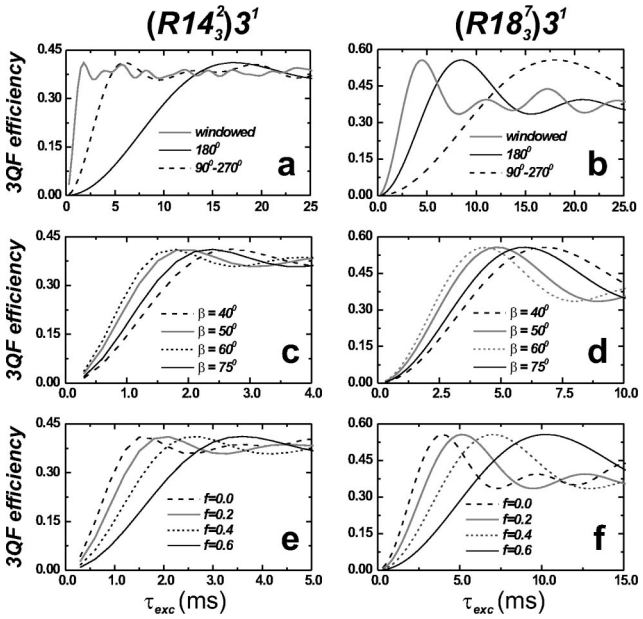

FIG. 3. Numerical simulations [based on Eq. (71)] of ^{13}C 3QF efficiency curves from a three-spin system in a powder spinning at $\omega_r/2\pi = 10.000$ kHz using $(R14_3^2)3^1$ (left column) and $(R18_3^7)3^1$ (right column). The calculations employed ^{13}C–^{13}C dipolar couplings of $^{13}C_3$–alanine but no chemical shift interactions. (a) and (b) curves obtained from different elements $\mathcal{R}$; two windowless elements $\mathcal{R}=\pi_0$ and $\mathcal{R}=(\pi/2)_0(3\pi/2)_\pi$ and a windowed one, $\mathcal{R}_w(\beta=55°)$ with pulse fraction $f=0.10$. Note that the latter provides higher scaling factors and thereby faster 3QC excitation. (c) and (d), 3QF efficiency curves from $\mathcal{R}_w(\beta)$ with $f=0.10$ for different angles β. In agreement with Eq. (77), the largest scaling factor is obtained for $\beta\approx 55°$. (e) and (f), same as in (c) and (d), but for constant $\beta=55°$ and variable pulse fraction f.

Reference or *numerically exact* simulations refer to first estimating a numerically exact propagator over the entire pulse sequence, followed by propagation of the density operator. Finally, a 3QF efficiency function, sampled in steps of T, was calculated from Eq. (73). Additionally, the AH governing the numerically exact propagator was determined. Then *either* its 3Q operators, *or* the sum of 3Q and ZQ operators were extracted (denoted *3Q-projected* or *3Q/ZQ-projected* exact AH, respectively) and used in subsequent calculations according to Eq. (73). This AHT approach includes all 3Q (or, alternatively all 3Q+ZQ) contributions to the average Hamiltonian to infinite order. Also, we performed analytical second order AH calculations based on the Hamiltonian in Eq. (72), assuming perfect behavior of the $\mathcal{S}3^1$ and $(\mathcal{S}\mathcal{S}')3^1$ MQ phase cycles, i.e., that only 3Q and ZQ dipolar terms contribute in the former case, and only 3Q terms in the latter. All other dipolar-deriving MQ contributions, as well as all other interactions, were ignored as they are symmetry forbidden. The validity of this approximation was confirmed by comparison with numerically exact reference calculations.

Comparing ''exact'' simulations with 3Q/ZQ-projected AH calculations shows how accurate AHT models the excitation dynamics, while comparing the 3Q/ZQ-projected AH and second order analytical simulations indicates the validity of truncating the Magnus expansion at second order, i.e., of using the approximation $\bar{H}\approx\bar{H}_{3Q}^{(2)}+\bar{H}_{ZQ}^{(2)}$.

B. 3Q scaling factors

Since the rate of 3QC excitation depends on the frequencies $\bar{\omega}_{T_r}^{(ij\times ik)}$, in turn proportional to the scaling factors $\kappa_{\substack{2m_2 22\\ 2m_1 21}}$, it is desirable to find combinations of pulse sequence symmetries and elements $\mathcal{E}^0$ giving the largest possible scaling factors. The main weakness with the second order recoupling approach is that the cross terms are in general small. In favorable cases, the dimensionless second order scaling factor $\kappa_{\substack{2m_2 22\\ 2m_1 21}} \sim 0.01$, typically an order of magnitude smaller than its first order counterparts $\kappa_{2m_2 22}$ and $\kappa_{2m_1 21}$. Further, in contrast to the first order recoupling case, the *second order dipolar frequencies* are inversely proportional to the spinning frequency [Eq. (29)].

Traditionally in first order recoupling applications, the elements $\mathcal{R}=\pi_0$ and $\mathcal{R}=(\pi/2)_0(3\pi/2)_\pi$ are employed for $\mathrm{R}N_n^\nu$ sequences[12,13,19,20,22,27,29] and $\mathcal{C}=(2\pi)_0$, $\mathcal{C}=(2\pi)_0(2\pi)_\pi$ and $\mathcal{C}=(\pi/2)_0(2\pi)_\pi(3\pi/2)_0$ in the case of $\mathrm{C}N_n^\nu$ schemes.[13,15,16,18,29,46] However, simulations show that these elements are generally nonoptimal for second order recoupling applications, as demonstrated by Figs. 3(a)–3(b). Instead, we have employed *windowed* $\mathcal{C}$ and $\mathcal{R}$ elements, providing larger first order dipolar scaling factors than the windowless options,[13,31,35] a property carried over and accentuated for the second order scaling factors. Two classes of windowed elements, internally compensated to isotropic chemical-shift interactions, are[13,31,35]

$$\mathcal{R}_w(\beta)=\{\beta_0-\tau_w-\pi_0-\tau_w-\beta_\pi\}, \tag{75}$$

$$\mathcal{C}_w(\beta)=\{\beta_0-\tau_w-\pi_0-\tau_w-(\pi-\beta)_0\}. \tag{76}$$

Here τ_w denotes a ''window'' interval, during which the rf fields are turned off, and timed such that the entire element extends over $\tau_E=n\tau_r/N$.

Equations (31) and (33) show that 3Q scaling factors have parts of the form $\kappa_{2m_2 22}\kappa_{2m_1 21}$; therefore, optimal second order scaling factors $\kappa_{\substack{2m_2 22\\ 2m_1 21}}$ result from recoupling sequences that simultaneously effect large 2Q *and* 1Q *first order scaling factors.* 2Q and 1Q scaling factors depend on the pulse flip angle β of the windowed element as $\kappa_{2m_2 22}\sim\sin\beta$ and $\kappa_{2m_1 21}\sim\sin 2\beta$, having optima at $\beta=\pi/2$ and $\beta=\pi/4$, respectively.[31] This predicts that their optimum product,

$$\kappa_{\substack{2m_2 22\\ 2m_1 21}}^{\approx} \kappa_{2m_2 22}\kappa_{2m_1 21}\sim\sin\beta\sin 2\beta \tag{77}$$

is obtained for $\beta=\theta_m\approx 54.7°$. These arguments are only approximate, as $\kappa_{\substack{2m_2 22\\ 2m_1 21}}$ depends also on $\kappa^{\Delta}_{\substack{2m_2 22\\ 2m_1 21}}$ [Eq. (30)], which is not directly related to the first order scaling factors. Nevertheless, the optimal angle β is in practice found within the range $50°\lesssim\beta\lesssim 60°$ as confirmed by the simulations shown in Figs. 3(c)–3(d). The scaling factors of windowed elements $\mathcal{E}^0$ also depend on the relative durations between the pulses and windows over τ_E,[31] reflected by the *pulse fraction f*,

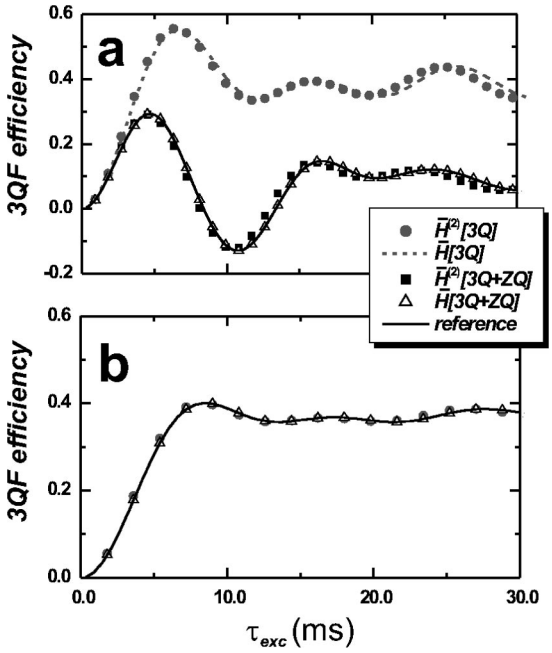

FIG. 4. Comparison of simulated ^{13}C 3QF curves obtained from the MQ-phase cycle $(\mathrm{R}18_3^7)3^1$ (a) and the corresponding MQ-phase inversion supercycle $(\mathrm{R}18_3^7\mathrm{R}18_3^{-7})3^1$ (b). The element $\mathcal{R}_w(50°)$ was employed with $f=0.30$ and other parameters as in Fig. 3. The solid lines correspond to numerically exact simulations and the others to excitation dynamics from various approximative average Hamiltonians (AH); the curves labeled $\bar{H}^{(2)}[3Q]$ were obtained from Eq. (71), including all recoupled 3Q terms listed in Table III, whereas $\bar{H}^{(2)}[3Q+ZQ]$ resulted after also including the recoupled ZQ terms. Curves labeled $\bar{H}[\cdots]$ implies calculations starting by numerically determining the AH (accurate to infinite order of the Magnus expansion), separating its contributions into various MQ operators, and only retaining the 3Q or 3Q+ZQ parts in the cases $\bar{H}[3Q]$ and $\bar{H}[3Q+ZQ]$, respectively.

$$f=\tau_E^{-1}\sum_{p=1}^{\text{pulses in }\mathcal{E}^0}\tau_p\,. \tag{78}$$

As shown by the simulations in Figs. 3(e) and 3(f), the scaling factor is maximized when f is minimized.

C. 3Q phase cycles versus 3Q phase inversion supercycles

From an ''ideal'' 3Q-recoupling sequence, we demand that (i) it is 3Q selective, i.e., effects an average Hamiltonian according to Eq. (71), with suppression of interfering dipolar terms to first and second order AHT; (ii) it provides the highest possible 3Q scaling factors; (iii) the recoupling is efficient over a large range of isotropic and anisotropic chemical shifts; (iv) it is robust to rf imperfections; and (v) operational over a wide range of spinning frequencies. We performed an extensive numerical search over potential $\mathcal{C}$ and $\mathcal{R}$ elements and (N,n,ν) symmetry numbers. The sequence found that best fulfill criteria (i)–(v) above is $\mathrm{R}18_3^7$, a 3Q/ZQ-selective class I sequence. It is further stabilized by the incorporation of MQ phase cycling and phase inversion supercycles. We therefore focus on evaluating $(\mathrm{R}18_3^7)3^1$ and $(\mathrm{R}18_3^7\mathrm{R}18_3^{-7})3^1$ by numerical simulations.

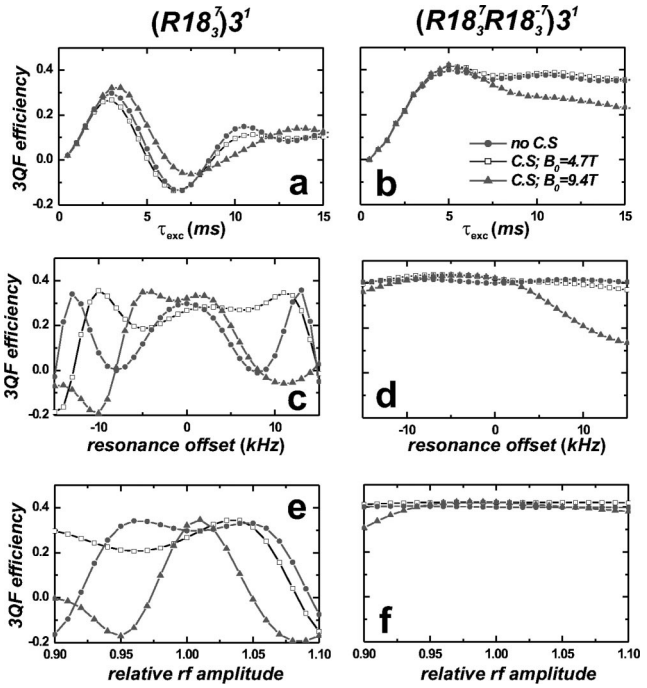

FIG. 5. Numerically exact simulations at $\omega_r/2\pi=6.000$ kHz of the response to chemical shift interactions (a)–(d) and deviations from the nominal value of the rf amplitude (e), (f) for $(R18_3^7)3^1$ (left column) and $(R18_3^7R18_3^{-7})3^1$ (right column). Calculations included either only $^{13}C-^{13}C$ dipolar couplings representative of alanine (circles) or additionally chemical shifts at 4.7 T (squares) and 9.4 T (triangles). $\mathcal{R}_w(50°)$ and $\mathcal{R}_w(60°)$ with $f=0.30$ were used for $(R18_3^7)3^1$ and $(R18_3^7R18_3^{-7})3^1$, respectively, giving $\omega^C_{\mathrm{nut,nom}}/2\pi=93$ kHz and 100 kHz. (a), (b) 3QF efficiencies as function of the excitation interval τ_{exc}. In (c)–(f), the 3QC excitation interval was fixed at $\tau_{\mathrm{exc}}=3.00$ ms (c),(e) and $\tau_{\mathrm{exc}}=5.00$ ms (d),(f). (c),(d), 3QF efficiencies as function of the resonance offset, defined as zero when the rf carrier frequency is set exactly in between the carboxyl and methyl ^{13}C sites. (e),(f), 3QF efficiencies as function of the ratio between the actual ^{13}C nutation frequency used and the nominal value $\omega^C_{\mathrm{nut,nom}}$.

1. Effects of zero-quantum terms

$\mathcal{S}3^1$ schemes are advantageous over $(\mathcal{SS}')3^1$ sequences in that they provide larger dipolar scaling factors and may effect γ-encoded 3Q recoupling by careful choice of symmetry numbers, as will be discussed elsewhere. Their most pronounced disadvantage is the unavoidable recoupling of ZQ terms that generally perturb the 3QC excitation dynamics significantly, resulting in 3QF efficiencies between 20–40 % in contrast to the theoretical 3QF efficiency of ≈55%.

Figure 4 compares various analytical and numerical strategies to approximate the Hamiltonian governing the 3QC excitation in the case of $(R18_3^7)3^1$ and $(R18_3^7R18_3^{-7})3^1$. Only dipolar couplings were included in the simulations; *J* couplings do not affect the 3QC dynamics in three-spin systems and the effects of chemical shift interactions will be considered in the next section. When only including the 3Q part of the second order average dipolar Hamiltonian, ≈55% 3QF efficiency is obtained from $(R18_3^7)3^1$ [Fig. 4(a)] in excellent agreement with the results from the 3Q-projected numerically determined AH. However, $(R18_3^7)3^1$ also recouples a set of ZQ terms (see Table III), in practice reducing the 3QF efficiency to ≈30% [Fig. 4(a)]: again there is excellent agreement with the results of the numerically calculated 3Q/ZQ-projected AH. Further, the latter simulation is indistinguishable from the numerically exact reference calculation. These results underline the excellent capabilities of the second order analytical AHT to account for the 3QC dynamics.

The theory predicts that $\overline{H}^{(2)}_{\mathrm{ZQ}}$ may be removed by employing phase inversion supercycling: this is confirmed by the numerical simulations of $(R18_3^7R18_3^{-7})3^1$. Figure 4(b) shows that the analytical calculations based on $\overline{H}^{(2)}_{\mathrm{3Q}}$, the 3Q/ZQ-projected AH simulations, and the numerically exact reference calculations all agree very well. Also, identical results (not shown) were obtained from $\overline{H}^{(2)}_{\mathrm{3Q}}+\overline{H}^{(2)}_{\mathrm{ZQ}}$ and the 3Q-projected numerically determined AH. These simulations show that the $(R18_3^7R18_3^{-7})3^1$ scheme suppresses all ZQ terms, but at a price of lowering the theoretical 3QF efficiency from ≈55% to about 40%. Nevertheless, the 3QF efficiency offered by the $(R18_3^7R18_3^{-7})3^1$ scheme is in practice higher than for $(R18_3^7)3^1$ due to the latter's undesirable ZQ contributions.

2. Effects of chemical shifts and Rf errors

In realistic scenarios, the dipolar recoupling should be reasonably robust to interference from chemical shift interactions as well as experimental imperfections, such as instabilities in the amplitudes and phases of the rf field during the application of the pulse sequences. Although the scheme $(R18_3^7)3^1$ is the best option found so far for 3Q recoupling, Fig. 5(a) shows that its 3QC dynamics is significantly perturbed by chemical shifts over longer time scales. The results correspond to powder averaged ^{13}C 3QF efficiencies predicted from numerically exact simulations for three cases: one solely dipolar coupling based (circles) and two including both isotropic and anisotropic chemical shifts, either at a magnetic field of 4.7 T (squares) or 9.4 T (triangles). Despite that chemical shifts are symmetry-forbidden and further locally suppressed over each R element,[31] the presence of ZQ terms of the AH magnifies the effects of residual shift terms and may lead to severe susceptibilities of the recoupling to chemical shift interactions.

These problems are partially circumvented by employing phase-inversion supercycling, as shown by the simulated 3QF efficiency curve of the corresponding sequence $(R18_3^7R18_3^{-7})3^1$ [Fig. 5(b)]. Nevertheless, the simulations of Fig. 5 indicate that an analysis of 3QF curves must consider chemical shift interactions explicitly to properly account for the observed dynamics, especially if geometric information about the spin system is to be extracted. These problems arise from the necessity to employ long excitation intervals τ_{exc}, requiring extremely high compensation to chemical shifts. This is also encountered in the determination of long-range internuclear distances by current state-of-the-art 2Q recoupling sequences.[18,20,27–29,46]

Figures 5(c) and 5(d) show the dependence of the rf carrier position (related to the robustness of a pulse sequence to a spread in isotropic chemical shifts among the spins) for $(R18_3^7)3^1$ and $(R18_3^7R18_3^{-7})3^1$ at τ_{exc} fixed to the 3QF maximum for each sequence. In the case of $(R18_3^7)3^1$ and assuming equal isotropic shifts of the spins, fluctuations of the 3QF

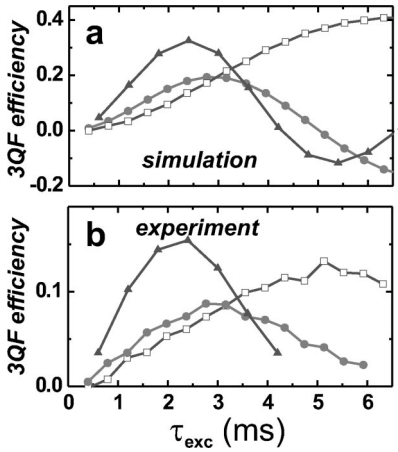

FIG. 6. (a) Numerically simulated and (b) experimentally acquired ^{13}C 3QF efficiency curves from a powder of dAla using $(R18_3^7)3^1$ and $(R18_3^7R18_3^{-7})3^1$ at 4.7 T. Curves with circles are results at $\omega_r/2\pi = 7.600$ kHz from $(R18_3^7)3^1$ [with $\mathcal{R}_w(57°)$ and $f=0.34$] whereas open squares represent $(R18_3^7R18_3^{-7})3^1$ [$\mathcal{R}_w(53°)$, $f=0.33$]. The triangles are results from $(R18_3^7)3^1$ [$\mathcal{R}_w(62°)$, $f=0.23$] at $\omega_r/2\pi=5.000$ kHz. All spin interactions were included in the simulations. Note the different vertical scales employed in (a) and (b).

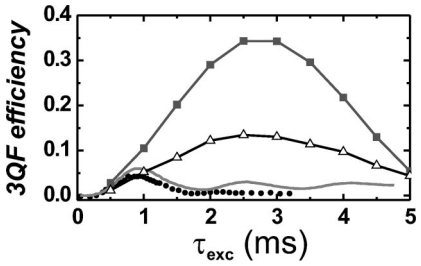

FIG. 7. Numerically simulated and experimentally acquired results of dAla at 9.4 T and $\omega_r/2\pi=6.000$ kHz, incorporating either the first order 2Q recoupling sequence POST-C7[9] or the second order 3Q recoupling scheme $(R18_3^7)3^1$ in 3QF experiments. POST-C7 converts 1QC into 3QC with a theoretical 3QF efficiency of ≈6.5% (Ref. 42) (gray line). Experimentally, 4.5% was obtained (circles). Considerably higher 3QF efficiencies were provided by applying $(R18_3^7)3^1$ directly to longitudinal magnetization; 34% and 13.5% were obtained numerically (squares) and experimentally (triangles), respectively.

efficiency curve are observed as the rf carrier is moved away from resonance, but a significantly enhanced robustness to frequency offsets results from using the $(R18_3^7R18_3^{-7})3^1$ sequence [Fig. 5(d)]. The chemical shift compensation may be improved for these schemes by increasing the spinning frequency or decreasing the pulse fraction by using more intense rf pulses.

Now considering effects from errors in the rf amplitudes, Figs. 5(e) and 5(f) indicate a strikingly enhanced robustness upon phase inversion supercycling to rf amplitude errors. The $(R18_3^7)3^1$ simulations display a very high susceptibility especially at the higher field of 9.4 T, whereas the 3QC dynamics obtained from the scheme $(R18_3^7R18_3^{-7})3^1$ is essentially unperturbed over a range of rf amplitudes within ±10% of the nominal value. In the case of $(R18_3^7)3^1$, the high sensitivity to the rf amplitude setting is likely to result from cross terms between chemical shifts and rf amplitude errors that are removed by the phase inversion cycle.[20,23,28]

VI. EXPERIMENTAL DEMONSTRATIONS

A. Samples and experimental conditions

3QF experiments incorporating $(R18_3^7)3^1$ and $(R18_3^7R18_3^{-7})3^1$ were conducted at 4.7 T and 9.4 T on Varian/Chemagnetics Infinity spectrometers. The experiments at 4.7 T were carried out on powders of 99% [U−^{13}C, ^{15}N] labeled L-alanine and L-tyrosine, using 4 mm rotors with ≈15 mg of samples restricted to the center 1/3 of the rotor volume to reduce rf inhomogeneity. The alanine sample was additionally isotopically ^2H labeled at the C^α (≈90%) and C^β (≈25%) positions, and is henceforth referred to as ''dAla.'' The experiments on dAla at 9.4 T were carried out with a 3.2 mm probehead.

The 3QF efficiencies were obtained by dividing the integrated spectral intensities resulting from the scheme in Fig. 1(f), with that of a conventional CPMAS experiment. All curves were sampled at completed $R18_3^7$ units. The proton nutation frequencies $\omega_{\mathrm{nut}}^H/2\pi$ employed during cross polarization and signal acquisition were typically ≈50 kHz and ≈90 kHz, respectively. TPPM decoupling[61] was used during the signal acquisition, whereas either conventional high power CW or amplitude-modulated decoupling (described in the supplementary material[50]) was applied throughout the ^{13}C recoupling sequences. Typically, $\omega_{\mathrm{nut}}^H/2\pi$ around ≈115 kHz and ≈215 kHz was used for the 4 mm and 3.2 mm probeheads, respectively. The numerically exact simulations employed spin interaction parameters of alanine listed in Ref. 62 and pulse parameters representative for the experimental values.

B. 3QF experiments

Figure 6 shows the 3QF efficiencies obtained from numerically exact simulations (a) and experiments (b) on dAla using $(R18_3^7)3^1$ at spinning frequencies of 5.000 kHz (triangles) and 7.600 kHz (circles); at the higher spinning speed results are also included from the supercycle $(R18_3^7R18_3^{-7})3^1$. The simulation at the lower spinning frequency predicts an optimum 3QF efficiency of 32.6% at $\tau_{\mathrm{exc}}=2.4$ ms and experimentally we obtained 15.4%. As the spinning frequency is increased to 7.600 kHz, both the simulations and experiments indicate a shift to a slightly longer optimal excitation interval, expected from AHT as the second order dipolar frequencies are inversely proportional to the spinning frequency. However, a drop in the simulated 3QF efficiency from ≈33% to 20% also occur, which may be traced to the corresponding increase of the pulse fraction from $f=0.23$ to $f=0.34$ upon the increase in ω_r: as the scaling factors of the 3Q and ZQ average Hamiltonian terms are dependent on the pulse fraction, their mutual interferences also change. Additionally, the $(R18_3^7)3^1$ sequence does not exhibit enough chemical shift compensation to be unperturbed when the pulse fraction increases. As expected, the supercycle $(R18_3^7R18_3^{-7})3^1$ effects a slower 3QC buildup than the $(R18_3^7)3^1$ scheme.

Generally, 3QF losses can be attributed to two main sources: rf inhomogeneity and interferences from $^1H-^{13}C$

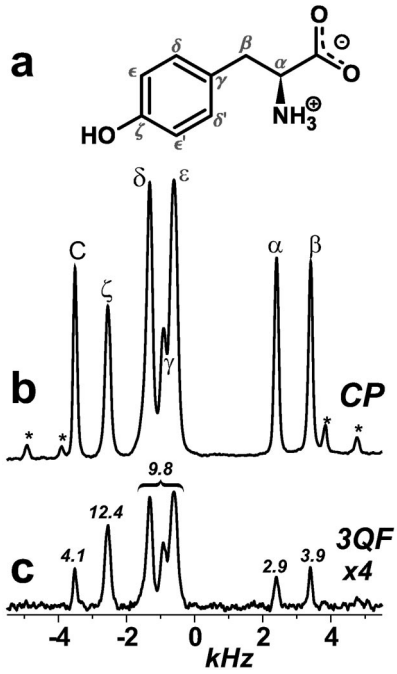

FIG. 8. (a) Molecular structure of L-tyrosine. (b),(c) Experimental ^{13}C spectra from a powder of [U−^{13}C, ^{15}N]−L-tyrosine at 4.7 T and $\omega_r/2\pi = 7.300$ kHz. (b) The result of a cross-polarization experiment, employing 1.5 ms contact time, 96 signal transients, 10 s recycle delay and 101 kHz TPPM decoupling (Ref. 61) during signal acquisition. The asterisks indicate spinning sidebands. (c) 3QF experiment, acquired under identical conditions as in (b) but also including a 3QF stage using $(R18_3^{\nu})3^1$ with $\mathcal{R}_w(51°)$; $f = 0.31$; $\nu = 7.005$; $\omega_{\mathrm{nut}}^C/2\pi = 110$ kHz; $\tau_{\mathrm{exc}} = \tau_{\mathrm{rec}} = 1.64$ ms; $\omega_{\mathrm{nut}}^H/2\pi = 110$ kHz and 117 kHz decoupling during ^{13}C pulses and windows, respectively, with ^1H rf phases given in the supplementary material (Ref. 50). The overall 3QF efficiency was 8.2%, and the percentage obtained from each ^{13}C site is given on top of each peak. The spectrum in (c) is displayed at 4 times magnification relative to that in (b).

couplings.[15,18,46] Nevertheless, besides from rather significant experimental 3QF losses, the qualitative features of the experimental curves match well those of the simulations, especially when considering the comparatively long excitation intervals involved. The main qualitative discrepancy is indeed occurring at larger values of τ_{exc}, most likely due to interferences from rf inhomogeneity. We also carried out 3QF experiments on a full rotor of dAla and only obtained 11% 3QF efficiency at $\omega_r/2\pi = 5.000$ kHz, amounting to

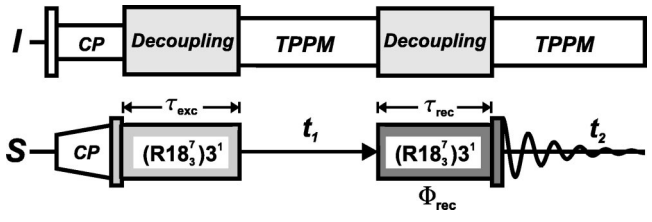

FIG. 9. Pulse scheme used for 3Q−1Q homonuclear correlation spectroscopy incorporating $(R18_3^7)3^1$ for 3QC excitation and reconversion. During t_1, 3QC evolve under chemical shift interactions, prior to their conversion into 1QC and the subsequent signal acquisition during t_2. After 2D Fourier transformation a spectrum is obtained that correlates the 3QC frequencies (along ω_1) with the corresponding 1QC frequencies (along ω_2) of each ^{13}C isotropic chemical shift.

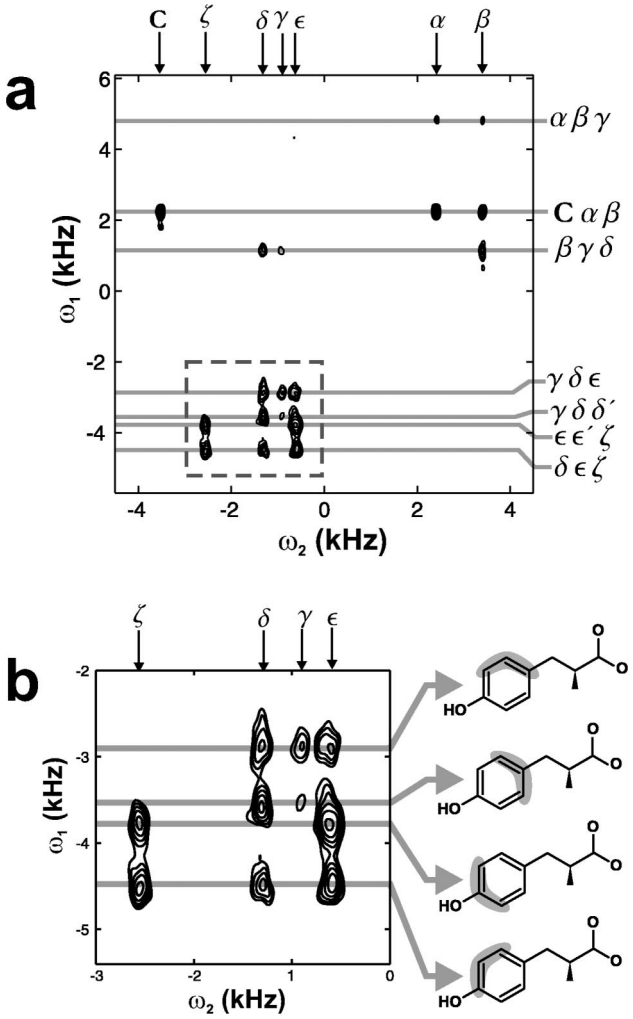

FIG. 10. (a) 2D 3Q−1Q correlation spectrum from [U−^{13}C, ^{15}N]−L-tyrosine at 4.7 T and $\omega_r/2\pi = 7.200$ kHz, using the pulse scheme of Fig. 9. The experimental parameters are as in Fig. 8, except $\tau_{\mathrm{exc}} = 1.67$ ms, $\tau_{\mathrm{rec}} = 0.83$ ms, $\omega_{\mathrm{nut}}^H/2\pi = 66$ kHz during ^{13}C pulses. (b) Zoom of the aromatic region [dashed box in (a)].

about 30% loss compared to the experiment on the restricted sample volume.

Figure 7 depicts the corresponding experiments and simulations of $(R18_3^7)3^1$ at $B_0 = 9.4$ T and $\omega_r/2\pi = 6.000$ kHz. As this probehead allowed using higher ^{13}C nutation frequencies, the pulse fraction employed at the higher spinning frequency was equal to that employed at $\omega_r/2\pi = 5.000$ kHz and 4.7 T. A similar 3QF efficiency of 13.5% was observed, indicating that no significant disturbances occurred from the increased chemical shift interactions at 9.4 T. Figure 7 also shows the results of a previously introduced 3QC excitation technique[42] relying on (first order) 2Q recoupling by POST-C7.[9] Comparing its experimental 3QF efficiency of 4.5% with that obtained by $(R18_3^7)3^1$ underlines the superior capabilities of 3Q recoupling in delivering efficient 3QC excitation in rotating solids; despite losses, the experimental results of 13.5% offered by $(R18_3^7)3^1$ is *twice that theoretically attainable by a 2Q recoupling sequence.*

The results of Fig. 8 demonstrate that $(R18_3^7)3^1$ may be successfully applied also to larger multiple-spin systems, in

this case [U−^{13}C, ^{15}N]-labeled L-tyrosine. A total of 8.2% 3QF efficiency was obtained at 4.7 T and $\omega_r/2\pi = 7.300$ kHz. The 3QF efficiency of the aromatic carbons amounts overall to more than 10%, while that of the alanine segment of the molecule is less than 4%. The intensities of the latter could not be significantly enhanced by using longer excitation intervals, which we attribute to strong interferences from the surrounding protons: as opposed to dAla, the entire ^{1}H dipolar network is intact in this sample. Additional discussion about heteronuclear decoupling in these experiments are provided in the supplementary material.[50]

C. Homonuclear 3Q–1Q correlation spectroscopy

A detailed discussion about various 2D correlation strategies employing 3QC and their structural information content will be given elsewhere. Here we only summarize the most important features of the 3Q–1Q correlation experiment.

A pulse scheme for 3Q–1Q correlation spectroscopy is depicted in Fig. 9. After a cross-polarization interval, longitudinal magnetization is obtained by a $\pi/2$ pulse. Next, 3QC is created by the $(\mathrm{R18}_3^7)3^1$ sequence of total duration τ_{exc}, corresponding to an arbitrary integer of completed $\mathrm{R18}_3^7$ blocks. Then follows an interval "t_1" during which each 3QC evolves under the sum of chemical shift interactions within each spin triplet. At the end of the interval, the 3QC has acquired a phase factor involving the sum of isotropic chemical shifts, $\exp\{it_1(\omega_i^{\mathrm{iso}}+\omega_j^{\mathrm{iso}}+\omega_k^{\mathrm{iso}})\}$ (disregarding CSA contributions). This frequency is generally unique to each 3QC and corresponds to the ω_1 coordinate in the 2D 3Q–1Q correlation spectrum. Next, the 3QC are reconverted into observable transverse magnetization by another sequence of $(\mathrm{R18}_3^7)3^1$ irradiation of duration τ_{rec} (not necessarily the same as τ_{exc}) followed by a $\pi/2$ pulse. This block of pulses is phase cycled to solely allow the coherence order transfer $\pm 3 \rightarrow -1$. The signal is subsequently acquired during "t_2."

Figure 10 shows the resulting 3Q–1Q ^{13}C correlation spectrum obtained from U–[^{13}C, ^{15}N]–L-tyrosine. As this molecule [Fig. 8(a)] comprise seven inequivalent ^{13}C nuclei, one expects in total seven different groups of 3QC signals in its 2D spectrum, if the 3QC excited only involves nuclei not separated by more than two bonds. These predictions are confirmed from the 2D spectrum. Note that for a given 3QC frequency in ω_1, one peak appears in the ω_2 dimension for each distinct spin, unless there are degeneracies in the chemical shifts, as in the case of $\mathrm{C}^{\zeta}-\mathrm{C}^{\epsilon}-\mathrm{C}^{\epsilon'}$. The only peculiar feature of the 2D spectrum of tyrosine is the $\mathrm{C}^{\alpha}-\mathrm{C}^{\beta}-\mathrm{C}^{\gamma}$ 3QC, for which the corresponding C^{γ} signal is missing in ω_2.

VII. CONCLUSIONS

By means of an extended second order AHT treatment of symmetry-based pulse sequences, we have designed 3Q recoupling schemes generating trilinear dipolar average Hamiltonians and applied them in the context of ^{13}C 3QC excitation in rotating solids. We obtained 15.4% 3QF efficiency in a powder of partially deuterated $^{13}\mathrm{C}_3$ L-alanine, and 8.2% in [U−^{13}C]–L-tyrosine. As about 2–3 times higher 3QF efficiencies are offered experimentally by the new approach compared to the previously best broadband technique,[42] comparable spectral S/N ratios are offered within an order of magnitude shorter experimental time. Alternatively, it allows application to larger molecular systems, although the 3QF efficiency delivered is still not high enough for large biomolecules. Nevertheless, the new approach may directly replace that of Ref. 42 as building block in experiments for estimating molecular torsion angles,[43] further combined with 2D correlation experiments for the measurement of multiple torsion angles as previously demonstrated by analogous 2Q experiments.[63] Other possibilities include tests for spin counting[45] and spectral editing by 3QF.[8]

The main inherent limitation with the second order based dipolar recoupling approach is the small sizes of the recoupled terms, making the recoupling susceptible to other interfering interactions such as chemical shifts. This is remedied partially by using windowed pulse elements that significantly enhances the second order dipolar scaling factors, provided that sufficiently strong rf pulses may be employed.

The theoretical aspects of this work extends previous treatments of symmetry-based pulse sequences[11–13,15–20,23,34] by (i) allowing a quick assessment of which terms are *decoupled* to second order AHT for MQ phases cycles and their combination with phase inversion supercycles and (ii) quantitative determination of the *remaining recoupled* second order terms. This may provide further insight into compensation mechanisms to interfering interactions in symmetry-based recoupling and decoupling schemes. Further, extensions to heteronuclear recoupling experiments by employing MQ phase cycles on dual rf channels[12] may be envisaged, as well as the engineering of higher-order MQ selective homonuclear recoupling sequences. The symmetry-based framework may also find applications outside the immediate scope of conventional recoupling and decoupling in MAS NMR, for example, in zero field NMR at high field[64] and in quantum information processing through solid state NMR.[65]

Further work is required to circumvent the problems with MQF losses in second order based recoupling experiments. However, this is motivated by the superior efficiencies they promise compared to recoupling techniques based on first order average Hamiltonians for high order MQC excitation.

ACKNOWLEDGMENTS

This work was supported by the Swedish Research Council (VR) and the Lars Hiertas Minne Foundation. We thank Malcolm H. Levitt for support and discussions, Zheng Weng for instrumental assistance, and Dick Sandström for providing the alanine sample.

APPENDIX: SECOND ORDER SCALING FACTORS FOR ARBITRARY PULSE ELEMENTS

Here the calculation of the factor $K^{m_2\lambda_2\mu_2}_{m_1\lambda_1\mu_1}$ in Eq. (37) is presented for an arbitrary pulse element $\mathcal{E}^0$, analogous to that of the first order case in Ref. 12. Assume that the element $\mathcal{E}^0$

is built of a sequence of $\mathfrak{N}$ rectangular pulses with flip angles and phases $(\xi_0)_{\phi_0},(\xi_1)_{\phi_1}\ldots,(\xi_{\mathfrak{N}-1})_{\phi_{\mathfrak{N}-1}}$ and rf nutation frequencies $\omega_{\mathrm{nut}}^0,\omega_{\mathrm{nut}}^1,\ldots,\omega_{\mathrm{nut}}^{\mathfrak{N}-1}$. The durations of the pulses are given by $\tau_0,\tau_1,\ldots,\tau_{\mathfrak{N}-1}$, where $\xi_p=\omega_{\mathrm{nut}}^p\tau_p$. Define the pulse Euler angles as follows:

$$\Omega_p=(A_p,B_p,G_p)=\left(\phi_p-\frac{\pi}{2},-\xi_p,-\phi_p+\frac{\pi}{2}\right). \tag{A1}$$

The factor $K_{\substack{m_2\lambda_2\mu_2\\ m_1\lambda_1\mu_1}}$ in Eq. (37) may be written as the sum of two parts resulting from the time integration over rectangular and triangular integration areas (similar to those shown in Fig. 2):

$$K_{\substack{m_2\lambda_2\mu_2\\ m_1\lambda_1\mu_1}}=K^{\square}_{\substack{m_2\lambda_2\mu_2\\ m_1\lambda_1\mu_1}}+K^{\triangle}_{\substack{m_2\lambda_2\mu_2\\ m_1\lambda_1\mu_1}}. \tag{A2}$$

The rectangular and triangular parts are given by

$$K^{\square}_{\substack{m_2\lambda_2\mu_2\\ m_1\lambda_1\mu_1}}=\sum_{p'=1}^{\mathfrak{N}-1}\frac{\tau_{p'}}{\tau_E}\tilde{K}^{(p')}_{m_2\lambda_2\mu_2}\sum_{p=0}^{p'-1}\frac{\tau_p}{\tau_E}\tilde{K}^{(p)}_{m_1\lambda_1\mu_1}, \tag{A3}$$

$$K^{\triangle}_{\substack{m_2\lambda_2\mu_2\\ m_1\lambda_1\mu_1}}=\sum_{p=0}^{\mathfrak{N}-1}\left(\frac{\tau_p}{\tau_E}\right)^2\tilde{K}^{(p)}_{\substack{m_2\lambda_2\mu_2\\ m_1\lambda_1\mu_1}} \tag{A4}$$

and the calculation of $\tilde{K}^{(p)}_{m\lambda\mu}$ is outlined in Ref. 12. The contributions $\tilde{K}^{(p)}_{\substack{m_2\lambda_2\mu_2\\ m_1\lambda_1\mu_1}}$ from the individual pulses are

$$\tilde{K}^{(0)}_{\substack{m_2\lambda_2\mu_2\\ m_1\lambda_1\mu_1}}=K^{(0)}_{\substack{m_2\lambda_2\mu_2\\ m_1\lambda_1\mu_1}},$$

$$\tilde{K}^{(1)}_{\substack{m_2\lambda_2\mu_2\\ m_1\lambda_1\mu_1}}=\exp\{i(m_2+m_1)\omega_r\tau_0\}\sum_{\mu_2',\mu_1'}D^{\lambda_2}_{\mu_2\mu_2'}(\tilde{\Omega}_0^{(2)})\times D^{\lambda_1}_{\mu_1\mu_1'}(\tilde{\Omega}_0^{(1)})K^{(1)}_{\substack{m_2\lambda_2\mu_2'\\ m_1\lambda_1\mu_1'}},\quad\ldots, \tag{A5}$$

$$\tilde{K}^{(p)}_{\substack{m_2\lambda_2\mu_2\\ m_1\lambda_1\mu_1}}=\exp\left\{i(m_2+m_1)\omega_r\sum_{p'=0}^{p-1}\tau_{p'}\right\}\times\sum_{\mu_2',\mu_1'}D^{\lambda_2}_{\mu_2\mu_2'}(\tilde{\Omega}^{(2)}_{p-1})D^{\lambda_1}_{\mu_1\mu_1'}(\tilde{\Omega}^{(1)}_{p-1})K^{(p)}_{\substack{m_2\lambda_2\mu_2'\\ m_1\lambda_1\mu_1'}}.$$

The terms $K^{(p)}_{\substack{m_2\lambda_2\mu_2\\ m_1\lambda_1\mu_1}}$ are given by

$$K^{(p)}_{\substack{m_2\lambda_2\mu_2\\ m_1\lambda_1\mu_1}}=\exp\{-i(\mu_2+\mu_1)A_p\}\times\tau_p^{-2}\int_0^{\tau_p}dt'\int_0^{t'}dt\,d^{\lambda_2}_{\mu_20}\left(B_p\frac{t'}{\tau_p}\right)d^{\lambda_1}_{\mu_10}\left(B_p\frac{t}{\tau_p}\right)\times\exp\{i\omega_r(m_2t'+m_1t)\}. \tag{A6}$$

The Wigner elements $D^{\lambda_2}_{\mu_2\mu_2'}(\tilde{\Omega}_p^{(2)})$ and $D^{\lambda_1}_{\mu_1\mu_1'}(\tilde{\Omega}_p^{(1)})$ are defined through the iterations

$$D^{\lambda_2}_{\mu_2\mu_2'}(\tilde{\Omega}_p^{(2)})=\sum_{\mu_2''}D^{\lambda_2}_{\mu_2\mu_2''}(\tilde{\Omega}^{(2)}_{p-1})D^{\lambda_2}_{\mu_2''\mu_2'}(\Omega_p), \tag{A7}$$

$$D^{\lambda_2}_{\mu_2\mu_2'}(\tilde{\Omega}_0^{(2)})=D^{\lambda_2}_{\mu_2\mu_2'}(\Omega_0), \tag{A8}$$

and

$$D^{\lambda_1}_{\mu_1\mu_1'}(\tilde{\Omega}_p^{(1)})=\sum_{\mu_1''}D^{\lambda_1}_{\mu_1\mu_1''}(\tilde{\Omega}^{(1)}_{p-1})D^{\lambda_1}_{\mu_1''\mu_1'}(\Omega_p), \tag{A9}$$

$$D^{\lambda_1}_{\mu_1\mu_1'}(\tilde{\Omega}_0^{(1)})=D^{\lambda_1}_{\mu_1\mu_1'}(\Omega_0). \tag{A10}$$

The case of smooth rf modulations may be handled by taking the limit of large $\mathfrak{N}$. Note that this calculation applies generally to any element $\mathcal{E}^0$ of pulses and windows, applied either once, or implemented periodically within the symmetry-based framework for $\mathrm{R}N_n^\nu$ or $\mathrm{C}N_n^\nu$ schemes.

[1] U. Haeberlen, in *High Resolution NMR in Solids. Selective Averaging*, edited by J. S. Waugh (Academic, New York, 1976).
[2] M. Mehring, *Principles of High Resolution NMR in Solids*, 2nd ed. (Springer-Verlag, Berlin, 1983).
[3] K. Schmidt-Rohr and H. W. Spiess, *Multidimensional Solid-State NMR and Polymers* (Academic, New York, 1994).
[4] A. E. Bennett, R. G. Griffin, and S. Vega, NMR Basic Principles Progr. **33**, 1 (1994).
[5] S. Dusold and A. Sebald, Annu. Rep. NMR Spectrosc. **41**, 185 (2000).
[6] W. S. Warren, D. P. Weitekamp, and A. Pines, J. Chem. Phys. **73**, 2084 (1980).
[7] J. Baum, M. Munowitz, A. N. Garroway, and A. Pines, J. Chem. Phys. **83**, 2015 (1985).
[8] M. Munowitz and A. Pines, Adv. Chem. Phys. **66**, 1 (1987).
[9] M. Hohwy, H. J. Jakobsen, M. Edén, M. H. Levitt, and N. C. Nielsen, J. Chem. Phys. **108**, 2686 (1998).
[10] M. Hohwy and N. C. Nielsen, J. Chem. Phys. **106**, 7571 (1997).
[11] M. Edén and M. H. Levitt, J. Chem. Phys. **111**, 1511 (1999).
[12] A. Brinkmann and M. H. Levitt, J. Chem. Phys. **115**, 357 (2001).
[13] M. H. Levitt, in Encyclopedia of NMR. Vol 9: Advances in NMR, 165 (2002).
[14] W. Magnus, Commun. Pure Appl. Math. **7**, 649 (1954).
[15] Y. K. Lee, N. D. Kurur, M. Helmle, O. G. Johannessen, N. C. Nielsen, and M. H. Levitt, Chem. Phys. Lett. **242**, 304 (1995).
[16] C. M. Rienstra, M. E. Hatcher, L. J. Mueller, B. Sun, S. W. Fesik, and R. G. Griffin, J. Am. Chem. Soc. **120**, 10602 (1998).
[17] J. D. Gross, P. R. Costa, and R. G. Griffin, J. Chem. Phys. **108**, 7286 (1998).
[18] M. Hohwy, C. M. Rienstra, C. P. Jaroniec, and R. G. Griffin, J. Chem. Phys. **110**, 7983 (1999).
[19] M. Carravetta, M. Edén, X. Zhao, A. Brinkmann, and M. H. Levitt, Chem. Phys. Lett. **321**, 205 (2000).
[20] M. Carravetta, M. Edén, O. G. Johannessen, H. Luthman, P. J. E. Verdegem, J. Lugtenburg, A. Sebald, and M. H. Levitt, J. Am. Chem. Soc. **123**, 10628 (2001).
[21] A. S. D. Heindrichs, H. Geen, C. Giordani, and J. J. Titman, Chem. Phys. Lett. **346**, 2142 (2001).
[22] X. Zhao, M. Edén, and M. H. Levitt, Chem. Phys. Lett. **342**, 353 (2001).
[23] A. Brinkmann, J. Schmedt auf der Günne, and M. H. Levitt, J. Magn. Reson. **156**, 79 (2002).
[24] P. K. Madhu, X. Zhao, and M. H. Levitt, Chem. Phys. Lett. **346**, 2142 (2001).
[25] J. C. C. Chan, Chem. Phys. Lett. **335**, 289 (2001).
[26] J. C. C. Chan and G. Brunklaus, Chem. Phys. Lett. **349**, 104 (2001).
[27] P. E. Kristiansen, D. J. Mitchell, and J. N. S. Evans, J. Magn. Reson. **157**, 253 (2002).
[28] T. Karlsson, J. M. Popham, J. R. Long, N. Oyler, and G. P. Drobny, J. Am. Chem. Soc. **125**, 7394 (2003).
[29] J. Schmedt auf der Günne, J. Magn. Reson. **165**, 18 (2003).
[30] M. Carravetta, J. Schmedt auf der Günne, and M. H. Levitt, J. Magn. Reson. **162**, 443 (2003).
[31] M. Edén, Chem. Phys. Lett. **378**, 55 (2003).
[32] E. H. Hardy, A. Detken, and B. H. Meier, J. Magn. Reson. **165**, 208 (2003).
[33] M. Bjerring and N. C. Nielsen, Chem. Phys. Lett. **370**, 496 (2003).

[34] Y. Matsuki, H. Akutsu, and T. Fujiwara, J. Magn. Reson. **162**, 54 (2003).
[35] M. Edén, Chem. Phys. Lett. **366**, 469 (2002).
[36] B. H. Meier and W. L. Earl, J. Chem. Phys. **85**, 4905 (1986).
[37] Y. Ba and W. S. Veeman, Solid State Nucl. Magn. Reson. **3**, 249 (1994).
[38] H. Geen, J. J. Titman, J. Gottwald, and H. W. Spiess, Chem. Phys. Lett. **227**, 79 (1994).
[39] U. Friedrich, I. Schnell, D. E. Demco, and H. W. Spiess, Chem. Phys. Lett. **285**, 49 (1998).
[40] H. Geen, R. Graf, A. S. D. Heindrichs, B. S. Hickman, I. Schnell, H. W. Spiess, and J. J. Titman, J. Magn. Reson. **138**, 167 (1999).
[41] C. Filip, M. Bertmer, D. E. Demco, and B. Blümich, Mol. Phys. **99**, 1575 (2001).
[42] M. Edén and M. H. Levitt, Chem. Phys. Lett. **293**, 173 (1998).
[43] M. Edén, A. Brinkmann, H. Luthman, L. Eriksson, and M. H. Levitt, J. Magn. Reson. **144**, 266 (2000).
[44] N. A. Oyler and R. Tycko, J. Phys. Chem. B **106**, 8382 (2002).
[45] C. E. Hughes, J. Schmedt auf der Günne, and M. H. Levitt, ChemPhysChem **4**, 457 (2003).
[46] A. Brinkmann, M. Edén, and M. H. Levitt, J. Chem. Phys. **112**, 8539 (2000).
[47] M. Edén, Concepts Magn. Reson. **17A**, 117 (2003).
[48] D. A. Varshalovich, A. N. Moskalev, and V. K. Khersonskii, *Quantum Theory of Angular Momentum* (World Scientific, Singapore, 1988).
[49] R. R. Ernst, G. Bodenhausen, and A. Wokaun, *Principles of Nuclear Magnetic Resonance in One and Two Dimensions* (Clarendon, Oxford, 1987).
[50] See EPAPS Document No. E-JCPSA6-120-004422 for supplementary material. A direct link to this document may be found in the online article's HTML reference section. The document may also be reached via the EPAPS homepage (http://www.aip.org/pubservs/epaps.html) or from ftp.aip.orq in the directory /epaps/. See the EPAPS homepage for more information.
[51] M. Carravetta, Doctoral dissertation, Stockholm University, 2002.
[52] A. Brinkmann (unpublished).
[53] A. Wokaun and R. R. Ernst, J. Chem. Phys. **67**, 1752 (1977).
[54] S. Vega, J. Chem. Phys. **68**, 5518 (1978).
[55] N. C. Nielsen, H. Bildsøe, H. J. Jakobsen, and M. H. Levitt, J. Chem. Phys. **101**, 1805 (1994).
[56] M. Munowitz, Mol. Phys. **71**, 959 (1990).
[57] O. W. Sørensen, J. Magn. Reson. **86**, 435 (1990).
[58] S. K. Zaremba, Ann. Mat. Pura. Appl. **4:73**, 293 (1966).
[59] H. Conroy, J. Chem. Phys. **47**, 5307 (1967).
[60] V. B. Cheng, H. H. Suzukawa, and M. Wolfsberg, J. Chem. Phys. **59**, 3992 (1973).
[61] A. E. Bennett, C. M. Rienstra, M. Auger, K. V. Lakshmi, and R. G. Griffin, J. Chem. Phys. **103**, 6951 (1995).
[62] M. H. Levitt and M. Edén, Mol. Phys. **95**, 879 (1998).
[63] V. Ladizhansky, C. P. Jaroniec, A. Diehl, H. Oschkinat, and R. G. Griffin, J. Am. Chem. Soc. **125**, 6827 (2003).
[64] R. Tycko, J. Chem. Phys. **92**, 5776 (1990).
[65] G. M. Leskowitz, N. Ghaderi, R. A. Olsen, and L. J. Mueller, J. Chem. Phys. **119**, 1643 (2003).